RAL-93-035

Science and Engineering Research Council
Rutherford Appleton Laboratory
Chilton DIDCOT Oxon OX11 0QX

RAL-93-035

The Laboratory Calibration of the Yohkoh Bragg Crystal Spectrometer

J Lang C M Brown J E Magraw and J Payne

July 1993

THE LABORATORY CALIBRATION OF THE YOHKOH BRAGG CRYSTAL SPECTROMETER

J. Lang[1], C. M. Brown[2], J. E. Magraw[1] and J. Payne[1]

[1] **Rutherford Appleton Laboratory, Chilton, Didcot, Oxon. OX11 0QX, U. K.**
[2] **Naval Research Laboratory, Washington, D. C. 20375, U. S. A.**

Abstract

The laboratory end-to-end testing of the Bragg Crystal Spectrometer (BCS) flown on the Japanese Yohkoh satellite is described. The details of the x-ray apparatus, the mounting and alignment of the BCS spectrometers and the tests carried out are presented. Results for the wavelength calibration and both relative and absolute efficiencies are given, with uncertainties. Appendices contain results of ancillary experiments pertinent to the calibration.

1. Introduction

The international consortium building the Bragg Crystal Spectrometer (BCS), which is a subsystem of the Japanese Solar A satellite (renamed Yohkoh after launch), agreed that the final testing of the experiment be carried out at the Rutherford Appleton Laboratory [RAL]. The crystals used to diffract the solar radiation had been thoroughly characterised (at the National Institute for Standards and Technology [NIST], Gaithersburg, Maryland, U.S.A.), the structures used to mount the crystals to receive the radiation had been designed, built and checked (at the Naval Research Laboratory [NRL], Washington D.C., U.S.A.) and the detectors and associated electronics box had been designed, built, tested and characterised (at the Mullard Space Science Laboratory [MSSL], U.K.). Even so the benefits of testing the spectrometers and electronics box after final assembly were clearly recognised. This final testing, the so-called end-to-end testing, since it involved shining suitable x-rays into the input end of the subsystem and checking the output at the subsystem spacecraft interface, consisted of a wavelength and spectral intensity calibration.

A description of the BCS scientific objectives and the flight apparatus is given in the paper by Culhane et al. (1991). The BCS observes in four separate wavelength ranges or channels. Each of the four channels has its own crystal, but the spectrometers (called BCS-A and BCS-B) are two-channel instruments, each carrying two of the crystals and having a single detector (with its high voltage unit) capable of serving two channels simultaneously. The details of the spectrometers including the desired wavelength ranges of the four channels and details of the crystals are given in table 1 for completeness. The wavelength ranges actually achieved depend on the Bragg angles built into the structure and the crystal bend radii.

This report contains a description of the end-to-end test apparatus (section 2), followed in section 3 by a description of the mounting and alignment of the BCS in the apparatus, and in section 4 by a brief outline of the BCS data handling and analysis system. Section 5 contains a description of the experimental method and the tests done. The wavelength calibration is given in section 6. Sections 7 and 8 contain the data and analysis for the relative and absolute intensity calibrations, respectively, and are followed by the conclusion section. Appendices give details of ancillary measurements needed to complete the laboratory characterisation of the experiment.

2. The apparatus

The end-to-end test apparatus is shown schematically in figure 1. Slits 1 and 2 were used to define a beam of x-rays emanating from an x-ray set. The channel-cut crystal was used to select the wavelength of the line to be used in the calibration. Slits 3 and 4, as well as being considered part of the channel-cut crystal monochromator, were also used in the alignment of the BCS spectrometers to the x-ray beam. The spectrometer being tested was

Table 1. BCS ion and crystal parameters and desired wavelength ranges

Channel number	1	2	3	4
Spectrometer	BCS-A	BCS-A	BCS-B	BCS-B
Desired upper wavelength (Å)	1.8044	1.8942	3.1912	5.1143
Desired lower wavelength (Å)	1.7636	1.8298	3.1631	5.0160
Ion	Fe XXVI	Fe XXV	Ca XIX	S XV
Resonance line wavelength (Å)	1.7780	1.8505	3.1773	5.0389
Crystal cut	Ge 220	Ge 220	Ge 220	Ge 111
Crystal 2d (Å)	4.000	4.000	4.000	6.532
Crystal measurements				
average length (cm)	18.08	18.11	11.35	11.34
average width (cm)	3.97	3.99	3.99	3.98
Bragg angle at resonance line (deg)	26.391	27.557	52.592	50.481
Bragg angle (deg),				
at desired upper wavelength	26.814	28.265	52.921	51.532
at desired lower wavelength	26.161	27.223	52.258	50.167
Desired Bragg angle range deg	0.653	1.042	0.663	1.365
mrad	11.40	18.19	11.57	23.82
Crystal rocking curve (arc sec fwhm)	14.0	14.2	36.4	79.3
Crystal integrated reflectivity (μrad)	65.41	66.85	113.8	156.8
Crystal bend radius (desired) (cm)	1588	995	986	478.5

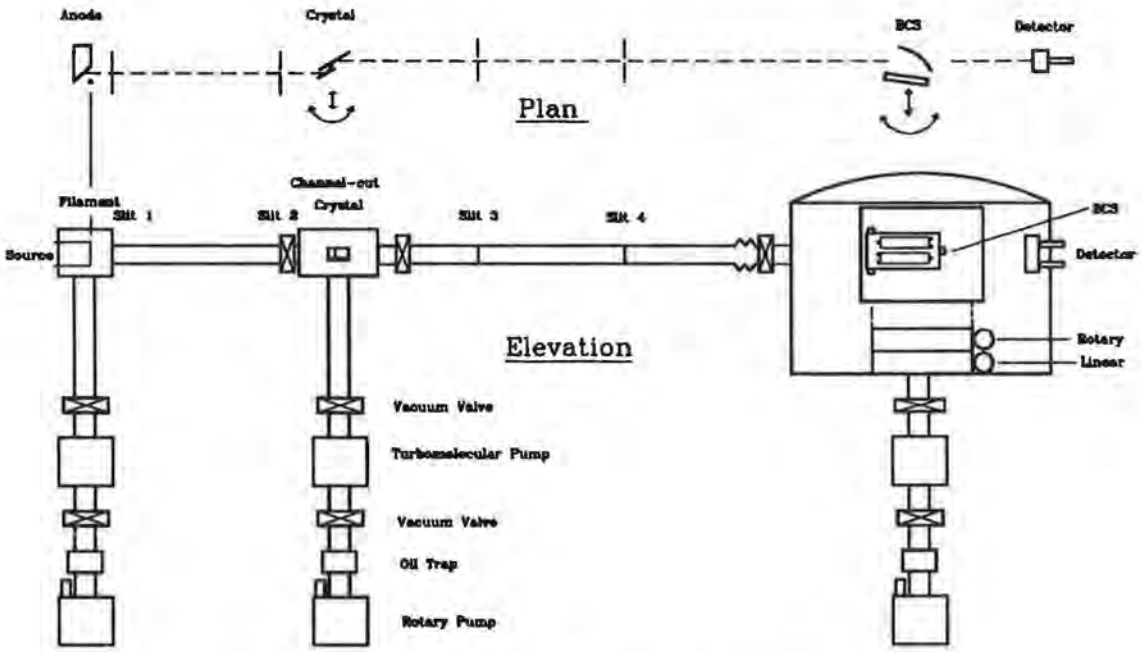

Figure 1. Schematic diagram of the end-to-end test apparatus

Table 2. Distances between the various components of the apparatus

Components	Distance/mm
Anode - first slit	70
First slit - second slit	490
Stop - crystal	90
Second slit - crystal	200
Crystal - third slit	420
Third slit - fourth slit	455
Fourth slit - detector	1180
Fourth slit - front of BCS	755

contained in a large vacuum chamber and could be translated and rotated with respect to the input x-ray beam. A direct beam detector was used as an x-ray monitor. Table 2 gives the horizontal distances between the various components.

Three identical turbomolecular pumping stacks were used to evacuate the system. Each of the three sections, the x-ray set with slits 1 and 2, the crystal chamber with slits 3 and 4, and the large test chamber could be isolated and evacuated separately. The x-ray set had a 50 mm long, vertically mounted, tungsten filament. The anode of commensurate size was water-cooled and made of either stainless steel or aluminium. The lines used were: channel 1, cobalt Kα; channel 2, holmium Lα; channel 3, calcium Kα; channel 4, molybdenum Lα. The Kβ line of calcium was also used for channel 3. To produce cobalt and molybdenum x-rays, a sheet of cobalt or molybdenum was attached to the anode using a conductive epoxy. For holmium and calcium, a pattern of holes 1 or 1.5 mm diameter at 2 mm centres was drilled in the central 50 mm by 15 mm area of the anode and the holes were packed with holmium oxide or chalk (calcium carbonate) respectively. A Spellman DXR3000 60 kV 3 kW power supply was used to run the x-ray set. This generator had an output voltage ripple of 0.01% for 10% line change and output voltage ripple of 0.1% RMS, stable to 0.02% per hour. The emission current stability was 0.02% per hour, regulated at 0.1% for a 50% voltage change. It was used mostly at 16 kV and at currents of up to 5 mA.

Slits 1 and 2 were 0.5 mm wide and 40 mm high. The reference optical axis for the system was defined using a laser beam directed through the effective centre of the anode and the centres of slits 1 and 2. The slits were adjusted to be vertical using a theodolite as a reference. The aperture stop was 43 mm high and 30 mm wide and was placed symmetrically about the optical axis to prevent radiation from the x-ray set passing around the crystal.

The monolithic channel-cut crystal was made of quartz cut to allow radiation to illuminate the $10\bar{1}1$ faces ($2d = 6.592$Å). Figure 2 shows the peak reflectivity of this cut of quartz as well as the single crystal rocking curve full-width half-maximum as a function of wavelength as obtained for the XRP SMM Flat Crystal Spectrometer (Kent 1988). The outside surfaces of the crystal were used to determine the cut of the crystal and are within 1 arc minute of the required direction. The surfaces of the leaves of the crystal were lapped to microgrit finish. The inner faces of the leaves of the crystal were parallel to each other to better than 10 microns. A drawing of the channel-cut crystal is shown in figure 3.

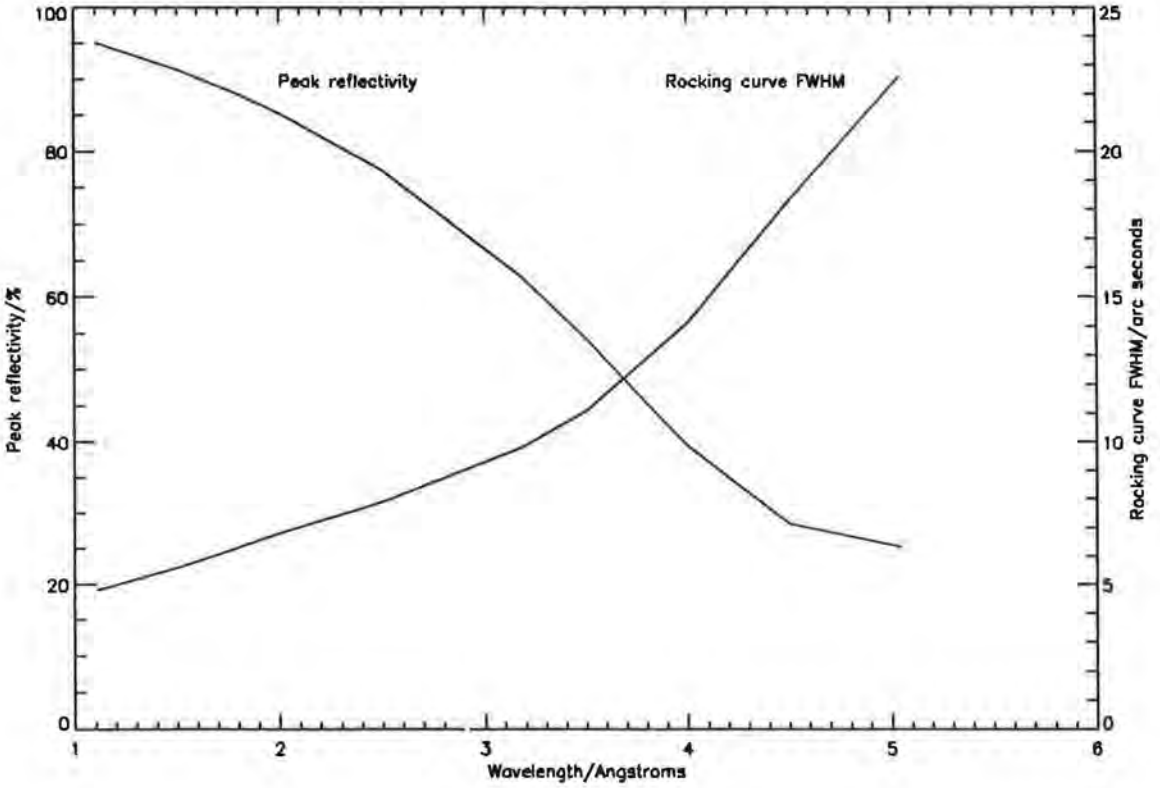

Figure 2. The single crystal peak reflectivity of quartz $10\bar{1}1$ as a function of wavelength

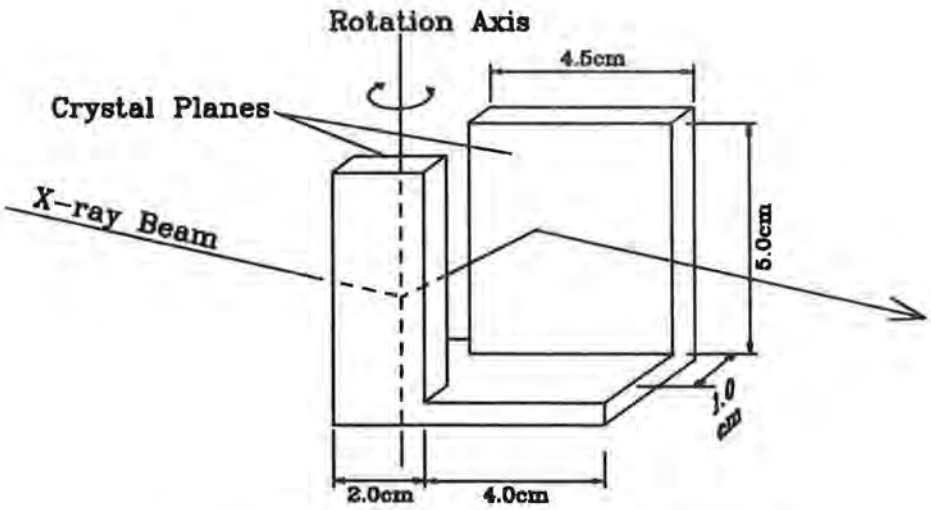

Figure 3. A drawing of the channel-cut crystal

The crystal, which was mounted in a holder with the leaves vertical, could be translated horizontally (perpendicular to the x-ray beam) and rotated from outside the vacuum chamber. The axis of rotation of the crystal was vertical and passed through the centre of

the inner face of the smaller leaf. The chosen wavelength then propagates through slits 3 and 4 parallel to the original beam, but with an offset that changes slightly as the channel-cut crystal is rotated. Table 3 gives the Bragg angles needed to allow the chosen lines to be reflected by the crystal and the corresponding offsets.

Table 3. The x-ray lines used, their Bragg angles and output beam offsets from the channel-cut crystal and the corresponding x-ray monitor window transmissions and gas efficiencies.

Line	Energy (keV)	Wave-length(Å)	Bragg angle(deg)	Offset (mm)	X-ray Monitor Window transmission	X-ray Monitor Gas efficiency
Co $K\alpha_1$	6.930	1.789	15.748	19.25	0.99±0.01	0.52±0.02
Co $K\alpha_2$	6.915	1.793	15.783	19.25		
Ho $L\alpha_1$	6.719	1.845	16.256	19.20	0.99±0.01	0.55±0.02
Ho $L\alpha_2$	6.681	1.856	16.351	19.19		
Ca $K\beta$	4.013	3.090	27.949	17.67	0.95±0.01	0.96±0.01
Ca $K\alpha_1$	3.692	3.358	30.626	17.21	0.94±0.01	0.98±0.01
Ca $K\alpha_2$	3.688	3.362	30.663	17.20		
Mo $L\alpha_1$	2.293	5.407	55.105	11.44	0.78±0.03	0.77±0.01
Mo $L\alpha_2$	2.290	5.415	55.224	11.41		

Slits 3 and 4 were set to be 40 mm high and adjusted to be vertical. The slits could be moved at right angles to the beam along a horizontal axis to match the offset of the beam from the crystal. The widths of the slits were set using feeler gauges. When using K lines a width of 200 microns was sufficient to allow the α_1 and α_2 lines just to be resolved. For the weaker $L\alpha$ lines the slits were set to be 1000 microns wide which allowed the $L\alpha_1$ and $L\alpha_2$ lines to be resolved. The direct beam detector was a one dimensional position sensitive proportional counter, fabricated by the Danish Space Research Institute. It had a 6μ-thick mylar entrance window which measured 90 mm long by 5 mm wide, and was mounted with the long dimension vertical to match the x-ray beam profile. The size of the window used was limited such that the vertical length of the window subtended the same vertical angle as the aperture of the BCS with respect to the x-ray beam. The dimensions of the counter gas volume were 110 mm long by 12 mm wide and 26 mm deep. A flowing mixture of 7.5% methane and 92.5% argon was used as the counter gas. The signals from the single wire resistive anode were processed by electronics and software provided by Bateman and Joyce (1990). The position of the incident x-ray is measured by the asymmetry between the pulses recorded at each end of the wire. The anode pulses were pre-amplified in a vacuum interface electronics box which was mounted on the tank as close as possible to the detector and which also contained the high voltage protection network for the counter. Following pre-amplification, the signals were passed to the main electronics module. This provided a standard pulse which was used as input to a

scaler/timer or ratemeter. At the data rates encountered in the present experiment (less than 1 kHz) no deadtime corrections were necessary for this output. Such counts were used as the x-ray beam monitor. The module also provided the signals necessary as input to the commercial ADC card (Metrabyte DAS-8) used to digitise the signals. The card was installed in a 386 20 MHz PC. The data capture software could run for a set time or until a preset total count was obtained. The stored data could be processed to provide position and pulse height spectra which could be windowed with user-defined thresholds and to provide a parameter file. The position spectra were used to monitor the distribution of x-rays along the height of the beam. As the height of the beam was chosen to match the width of the BCS crystal, any gross non-uniformity in the beam would mean that parts of the crystal/detector combination might be relatively over- or under-exposed to x-rays and cause bias in the measurements. The variations in intensity along the beam were usually less than ±25% of the mean intensity. Figure 4 shows a typical position histogram taken when the channel 4 wavelength calibration was being done. Figure 5 shows the x-ray monitor signal obtained by rotating the crystal when the x-ray set was run to produce cobalt Kα radiation and slits 3 and 4 were set to be 200 microns wide. The weaker α_2 line is resolved from the α_1 line. Also shown in figure 5 are the results of a similar scan over the holmium Lα lines with slits 3 and 4 set at 1000 microns. The much weaker α_2 line is clearly resolved.

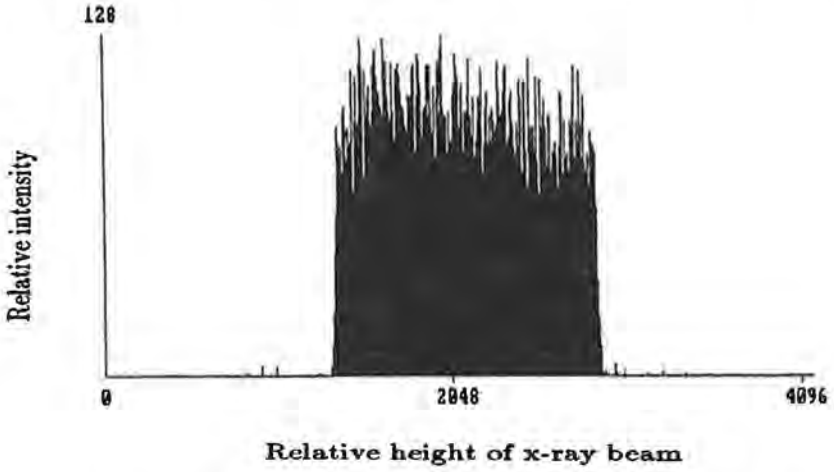

Figure 4. An x-ray monitor histogram spectrum taken with a Mo Lα beam.

3. The mounting and alignment of the BCS.

So that the length of the x-ray beam would lie along a line parallel to the width of a BCS crystal, the BCS had to be mounted with the plane of the surfaces of its mounting feet vertical. Moreover, this plane could be to the west or east of the x-ray beam which propagated from north to south in the laboratory. With the feet mounted to the west ("feet west"), the channel-cut and the BCS crystals were in the (1, -1, -1) configuration, whereas

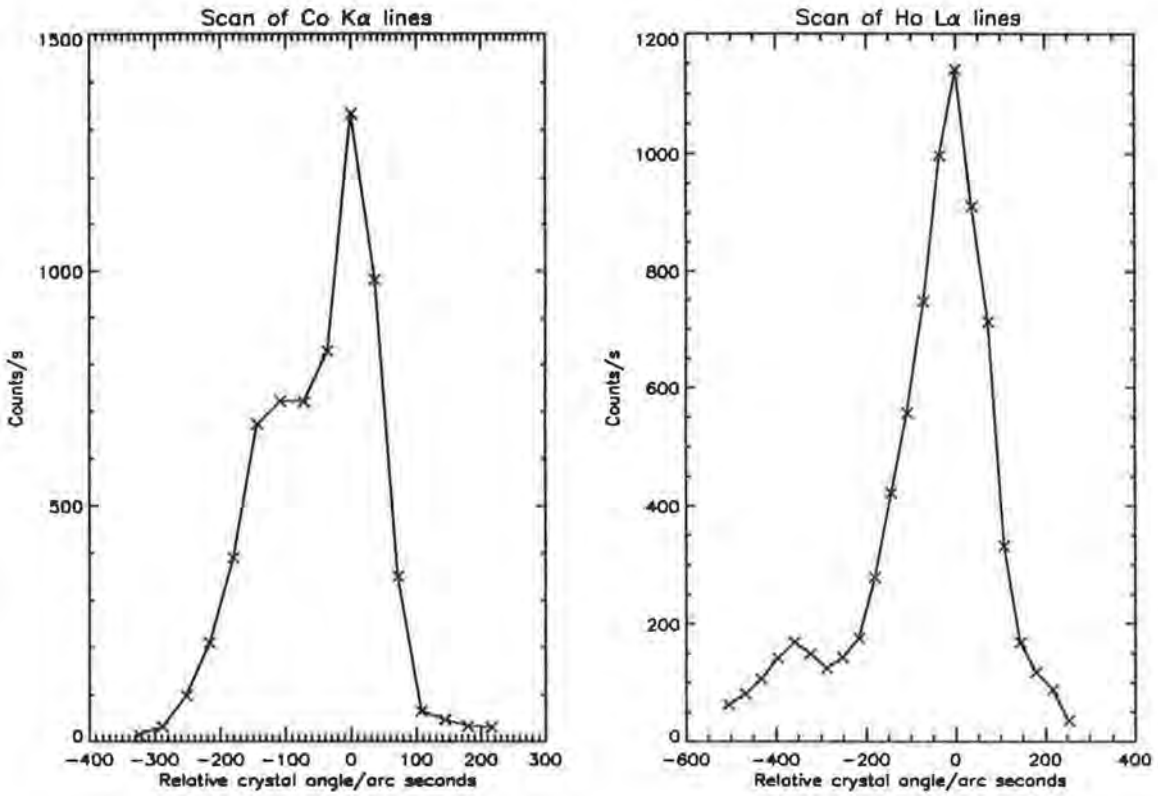

Figure 5. The x-ray monitor signal as a function of crystal rotation angle obtained for Co Kα and Ho Lα x-rays.

with the feet mounted to the east ("feet east") the configuration was (1, -1, 1). As shown in figure 1 the BCS can be moved in an east-west (x) direction allowing the x-ray beam to be scanned over the aperture of the BCS and also allowing the BCS to be pulled out of the beam to permit the x-ray monitor proportional counter to be used. This motion was driven by a stepping motor giving accurate reference positions at a rate of one step per micron, achieved using a Unidex 11 two-axis motion controller with an ATYS206/HM linear positioning stage. The other motion (y) of the controller (AOM130-6M) was used to rotate the BCS about a vertical axis. For BCS-A the rotation axis passed through a point 175 mm above the plane of the feet and 134 mm behind the entrance surface of the spectrometer such that the axis was 45 mm behind the centre of the crystal. For BCS-B the axis of rotation passed through a point 150 mm above the plane of the feet and 88 mm behind the plane of the entrance aperture, such that the axis was 29 mm in front of the centre of the crystal. This rotation was in steps of 0.125 arc seconds with repeatable accuracy of 0.375 arc seconds.

Neither the BCS detector nor the direct beam monitor could be used while any stepping motors were running because of electrical interference. However, during experiments the controller could be left energised to allow monitoring of the x and y positions. Checks were carried out with the Unidex controller turned on and off to assess the effects of any interference on the position spectra. No significant effects were found.

The first step in aligning the BCS to the x-ray beam was to determine the position of the x-ray beam. With the required anode in the x-ray set, slits 3 and 4 withdrawn from the beam and the direct beam monitor at the correct offset, the channel-cut crystal was rotated in fine steps around the known setting for the line to maximise the signal in the monitor. Then slits 3 and 4 (set at 200 microns) were put back. Each, in turn, was scanned laterally through the beam and locked in position where the monitor signal was maximum. Dry nitrogen was admitted to the tube containing the slits and to the large vacuum tank to bring them to atmospheric pressure. A beam from a He-Ne laser was then shone through the centres of slits 3 and 4 to verify that the direct beam monitor was correctly positioned.

The next step was to attach the BCS to its cuboid mounting box and locate it in the vacuum tank. This box was four-sided, having the two sides perpendicular to the beam missing to allow the BCS to view the x-ray beam and to allow the x-ray beam to reach the direct beam monitor. The two vertical sides were drilled with mounting holes, one set for BCS-A and the other for BCS-B. An optically aligned drill template was used to locate accurately the foot points of the BCS units in the cuboid. The BCS unit under test was then attached to the appropriate BCS-A or B side. The box was designed and checked after manufacture for mechanical accuracy such that if BCS-A was mounted feet facing west and then rotated 180 degrees about the x-ray beam direction the feet were still in the same vertical plane, but facing east. The box was positively located on the moving stages. When the box was turned over to change from say feet west to feet east and it was desired to view the same channel, a precision vertical spacer had to be introduced or removed; otherwise, on changing the BCS over, the other channel would be in the beam. This system allowed measurements to be made of both channels of each BCS unit in both the (1,-1,1) and the (1,-1,-1) orientation.

With the BCS located in the tank, an alignment mirror was attached to its aperture. This mirror had been prepared during the original setting up of the spectrometer structure such that a beam reflected from the mirror using, say an autocollimator, would define the spacecraft z axis (the sunward axis) to ±10 arc sec. The He-Ne laser beam previously aligned through the centres of slit 3 and 4 was reflected off this mirror. A piece of translucent graph paper was placed on the BCS side of slit 4 as close as possible to the slit, thus maximising the distance from the alignment mirror. The laser beam was adjusted so that it went slightly "downhill" such that the beam incident on the alignment mirror just grazed the top of the graph paper while the reflected beam fell just on the paper. By rotating the BCS, the input and output beams could be made to coincide horizontally. The input beam was a spot just after slit 4, while the reflected beam appeared as a diffraction pattern with a lozenge-shaped central maximum, about 8 mm wide. The BCS was considered aligned when the spot was just above the centre of the lozenge. A magnifying glass was helpful in viewing the alignment pattern. The limit of discernible motion of the lozenge was found to be 80 steps of the Unidex y rotation (i.e. 10 arc seconds) and 0.5 mm on the graph paper was 16 arc seconds. When Lα lines were to be used, slits 3 and 4 were widened symmetrically after alignment. The use of the wider slits during the optical alignment procedure was avoided since it resulted in lower precision.

4. The BCS data handling and analysis system

The BCS was commanded using its Electrical Ground Support Equipment (EGSE) which consisted of a spacecraft simulator controlled by a second 386 20 MHz PC which in turn had an ethernet link to a Microvax 3100 used for data analysis. Software on the PC allowed the BCS to be turned on and data taken for a specified interval. These data were stored on the Microvax and the health of the BCS and the acquired data could be monitored in real time on the PC. The files on the Microvax were time stamped and an added comment line allowed the Unidex position information to be recorded.

5. The experimental method and the observations

The performance of the spectrometer being tested was monitored at the beginning and end of each working day by running a standard BCS calibration routine which utilised the BCS internal radioactive source and detector stimulators.

For a particular configuration, measurements of a spectrometer channel were made with the feet mounted both west and east. The measurements with the feet east were less comprehensive than those with the feet west but necessary to provide data on the effects of having the BCS crystals in the 1 and -1 positions with respect to the channel-cut crystal. A calibration run with the feet west commenced with an alignment as discussed above. The counts in the x-ray monitor were recorded for one minute. Then, for the aligned y rotation position, the translation position at which the x-ray signal was maximum was found. This essentially gives the data for the wavelength calibration. A quick scan of the system was made by finding the peak signal rotations for about ten positions across the crystal aperture. This procedure was extended in both directions until the signal disappeared because the incident x-rays did not hit either the crystal or the detector. A plot of these crude numbers gave a "road map" of approximate x and y co-ordinates where the peak intensity of the beam could be found over the length of the BCS crystal, and was used to select appropriate positions for subsequent calibrations. Then resetting to the optically aligned y position and corresponding x position, an angle scan in y was done in 200-step (25 arc second) increments from the peak out to one side. Once the signal decreased significantly the step size was increased. When the signal fell to near zero, the y was reset and the scan restarted from the other side of the line, increasing y to the peak and then two increments beyond. Such angle scans were sometimes done at one or two additional positions away and on either side of the aligned y position. Between such scans, the signals at three standard positions on the BCS crystal, one at the x position of maximum signal for the aligned y rotation position and two at one increment in x (usually 0.5 or 1 mm) to each side of the maximum, were measured as a beam monitor, called hereafter a y monitor. Note that this is a different monitor from the direct beam x-ray monitor, for which it was necessary to move the BCS out of the beam, and which was also measured periodically (but less frequently) during the run. The relative intensity calibration was done by rescanning in x at the aligned y position and then incrementing y by a fixed

amount and scanning in x, then checking the y monitor and doing the next y increment, scanning x, then a y monitor check and so on till the whole aperture had been scanned. Then the x-ray direct beam monitor was checked, the apparatus let up to atmospheric pressure using dry nitrogen and the optical alignment rechecked. The scans with the feet east were less comprehensive, the relative intensity calibration scan not being necessary. All the BCS data were passed to the Microvax computer, analysed and archived. A descriptive log of the work was kept in a computer file. Also kept were summary files of the observations giving the filename (i.e. date and time), the bin number of the peak of the detector signal, the duration of the measurement, the count rate and details of the x and y positions. Table 4 gives details of the sets of observations made. For spectrometer BCS-A, both non-flight and flight crystals were tested as well as non-flight and flight detectors. In fact the non-flight detector was originally intended for flight but failed in vibration testing. Now that the satellite has been successfully launched the descriptions of results will be restricted to tests on flight equipment. The results of tests on non-flight equipment are available if required.

Table 4. Summary of tests done

BCS	Channel	Crystal	Detector	Feet	X-ray lines
A	1	non-flight	non-flight	west, east	Co K
A	2	non-flight	non-flight	west, east	Co K
A	1	flight	non-flight	west, east	Co K
A	2	flight	non-flight	west, east	Ho L
A	1	flight	flight	west, east	Co K
A	2	flight	flight	west, east	Ho L
B	3	flight	flight	west, east	Ca K
B	4	flight	flight	west, east	Mo L

6. The wavelength calibration

It is convenient to consider each spectrometer in turn as the x-ray lines used to calibrate spectrometer BCS-A lay within the solar wavelength ranges of A while those used for spectrometer BCS-B did not. It was assumed that for all channels the position encoded length of a detector was 256 bins wide. The flight software can read the encoded length of the channels at lower resolution and usually in flight operations BCS-B is set to a width of 128 bins.

6.1 Spectrometer BCS-A

Table 5a gives a summary of the results. For each channel, wavelength calibrations were done for both feet west and east. For all four cases the alignment position was found and

Table 5. Wavelength calibration

a. Data for BCS-A

Chnl	Feet	Alignment position (y steps) Before	After	Mean	Bin	Gradient (bins/step)	Corrected bin
1	W	203278.5	202978.5	203128.5	103.6±0.2	$8.293\ 10^{-3}$	102.4±2.0
1	E	202678.5	201978.5	202328.5	97.1±0.2	$8.293\ 10^{-3}$	100.0±3.0
2	W	202978.5	203228.5	203103.5	175.8±0.3	$5.913\ 10^{-3}$	176.5±2.0
2	E	202978.5	203278.5	203128.5	177.0±0.3	$5.913\ 10^{-3}$	176.1±2.0

(The standard deviation of the gradients for channel 1 and 2 are 0.6% and 0.5% respectively.)

b. Data for BCS-B

Chnl	Feet	Alignment position (y steps) Before	Mean	Bin	Position	Gradient (bins/step)	Corrected bin
3	W	128509.5	128679.5	105.1±0.5	258311.5	$1.027\ 10^{-2}$	103.4±2.0
3	E	13849.5	-	101.7±0.5	4049.5	$1.027\ 10^{-2}$	103.5±2.0
4	W	103600.5	103500.5	126.0±0.5	246867.0	$5.381\ 10^{-3}$	126.5±2.0
4	E	202700.5	202500.5	131.0±0.4	59532.5	$5.381\ 10^{-3}$	129.9±2.0

(The standard deviation of the gradients for channel 3 and 4 are 0.8% and 0.7% respectively.)

average alignment y0 value calculated. A scan across the crystal at different fixed y and scanning a range of x yielded a value of bins per step in y from the gradient of the graph of bin number for peak signal versus rotation. This gradient was used to correct the bin to the average alignment y position. Since the before and after measurements gave the bin position at the before and after rotation, the gradient was used to find the bin position at which the signal would have been received if the average rotation position had been used.

For channel 1 feet west, in estimating the uncertainty, it was noted that the optical alignment positions were ±150 steps i.e. ±1.24 bins on either side of the mean and that the alignment mirror and limit of discernible motion were ±0.66 bins each. Thus a value of ±2 bins is a reasonable uncertainty estimate for the feet west case. For the feet east case an uncertainty of ±3 bins is reasonable. The average of these measurements gives a value of bin 101±2 for the location of the peak of the Co Kα line for x-rays propagating parallel to the instrument axis, i.e. the spacecraft z axis. From the table of measurements of bin

positions and widths as a function of position on the detector window (Fludra, Phillips and Trow 1990), the bin position was converted to a physical location on the detector. Then a precision drawing package on a computer was used to estimate the wavelengths and uncertainties of the lowest and highest bins as given in table 6. The input to the drawing package included the precise location of all the components of the spectrometer as well as an allowance for the tilt of the crystal planes with respect to the physical surface of the crystal.

Table 6. Wavelength calibration results

Channel	Desired wavelength range (Å)	Bin range	Measured wavelength range (Å)
1	1.7636 - 1.8044	212 - 28	1.7597 - 1.8121 (±0.0006)
2	1.8298 - 1.8942	224 - 36	1.8284 - 1.8957 (±0.0007)
3	3.1631 - 3.1912	27 - 229	3.1633 - 3.1933 (±0.0003)
4	5.0160 - 5.1143	40 - 234	5.0163 - 5.1143 (±0.0015)

For channel 2, the uncertainties were assigned following a similar analysis as for channel 1. The average of the feet west and east measurements is 176±2 bins for the peak position of the holmium $L\alpha_1$ line. The procedure outlined for channel 1 yielded the results for the wavelengths of the highest and lowest bins as given in table 6.

6.2 Spectrometer BCS-B

For spectrometer BCS-B, no x-ray anode could be found that gave strong x-ray lines within the normal wavelength range of the channels, so once the alignment position had been found, an extra rotation was needed to bring the spectrometer to a suitable Bragg angle. Table 5b gives a summary of the results including the y rotation position in steps corresponding to the bin at which the signal peaked.

For channel 3 with the feet west, the tests included moving slits 3 and 4 to allow Ca Kβ to be observed. After the feet east test the optical alignment was not checked. The correction applied to the bin position for this case was obtained by comparing the difference between the (mean) alignment position and the rotation necessary to observe the line. The uncertainties were assigned after an analysis as for spectrometer BCS-A. The mean of the feet west and east cases was then used as described for spectrometer BCS-A to evaluate the wavelengths corresponding to the highest and lowest bins as given in table 6. Due allowance was made for the additional rotation.

For channel 4 when the first measurements were made, including the aperture scan from which the gradient (bins/step) is derived, it was noticed that the wavelength calibration was different from that expected. Two attempts were made to correct this by shimming. The preferred solution was found for a 0.022 inch shim at the end of the crystal with the

single mounting foot. This foot is at the long wavelength end of the crystal and the change resulted in about a 0.018A decrease in the wavelengths covered by channel 4. From the results given in table 6, the average of the feet west and east measurements gives bin 128± 3. Analysing the results for channel 4 in the same way as was done for the other channels gives the wavelengths corresponding to the highest and lowest bins as given in table 6.

6.3 Refractive index correction

Bragg's law for the diffraction of x-rays is

$$m\lambda = 2d \sin \theta_0 \qquad (1)$$

where λ is the wavelength, d the crystal lattice spacing, θ_0 a nominal angle of incidence and m the order of diffraction. Because of refraction of the x-rays as they pass into a crystal, equation 1 is corrected as follows

$$m\lambda = 2d \sin (\theta_0+\Delta) \qquad (2)$$

where $\Delta = \delta \sec \theta \operatorname{cosec} \theta$ is the refractive index correction, a small angular offset. $\delta = 1 - n$ and n is the refractive index. For germanium, δ/λ^2 is (almost) independent of λ except in the neighbourhood of absorption edges.

The calculated offsets Δ are given in table 7. As the wavelength range of each channel is small (see table 1), the offset is considered to be a constant for each channel. In any calculation it can then be added to the similar correction for the small angle between the crystal surface and the actual crystal planes. The only potentially noticeable effect comes in channel 4, where an approximate difference of 1 arc minute occurs between the Cu Kα radiation which was used at NIST to set up the crystal angles and the much softer S XV radiation. Again, this is well within the error budget for the channel 4 wavelength range.

Table 7. Refractive index correction for relevant BCS X-rays (from Cowan (1991) and Brennan and Cowan (1992))

Line	Energy (eV)	Wavelength (Å)	Crystal cut (Ge)	$\theta_0+\Delta$ (deg)	Δ (arc seconds)
Fe XXVI	6965	1.780	(2 2 0)	26.42	9.8
Fe XXV	6701	1.850	(2 2 0)	27.55	10.3
Ca XIX	3904	3.176	(2 2 0)	52.54	25.3
S XV	2450	5.061	(1 1 1)	50.77	62.4
Cu Kα	8048	1.541	(2 2 0)	22.65	8.2
Cu Kα	8048	1.541	(1 1 1)	13.64	12.8

7. The relative intensity calibration

7.1 Channel 1

For channel 1 figure 6 shows the six measured scans taken (feet west) across the aperture of the instrument to determine the relative intensity calibration. As discussed earlier, each scan was taken at a different y rotation. Not shown in the figure are the scans at the y monitor position which were taken at the wavelength calibration y rotation. Table 8 gives

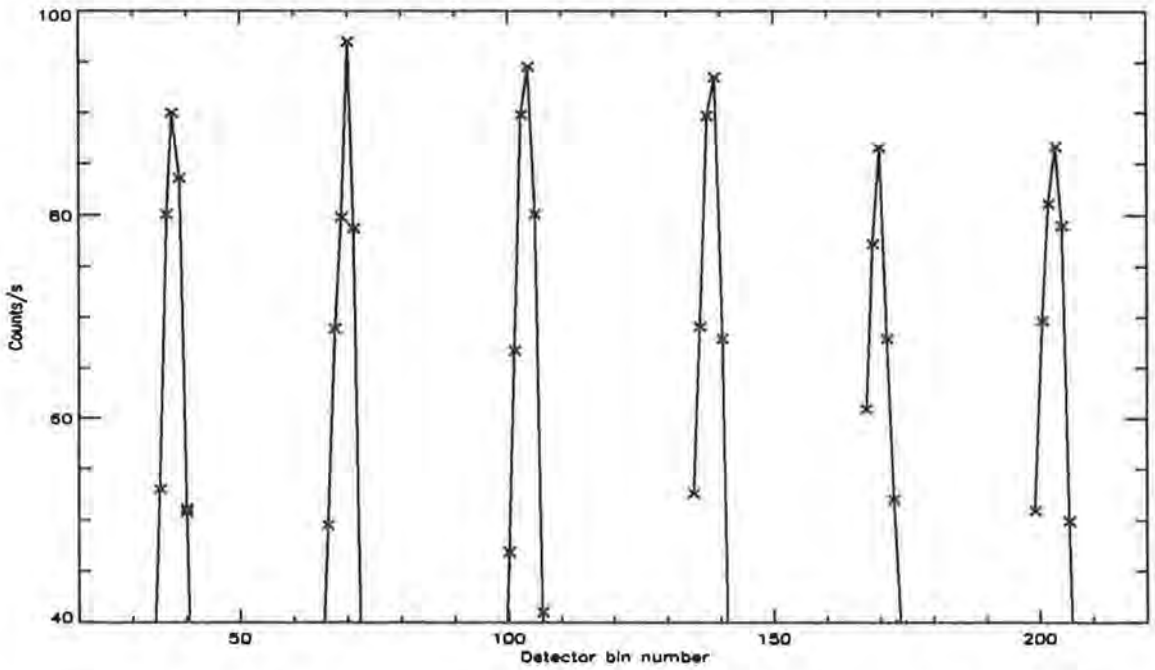

Figure 6. The scans taken across the aperture of BCS-A to determine the relative intensity calibration

a summary of the various measurements. The monitor scans are indicated by an additional m in the first column. The y monitor measurements allowed any drift in the output of the x-ray set as a function of time to be detected and accounted for. The time of observation and the x-ray monitor readings (counts in 10 seconds) with their mean and standard deviation are tabulated. Also given in the table are the x positions of the peaks of the scans in figure 6, the corresponding y rotation (where y0 indicates a y monitor scan; y0 = 203278.5 steps), the count rate from the spectrometer and the total counts. As the y monitor scans were repeated over the same three positions, the area under the curve of the plot of counts/s versus bin number was taken as the monitor signal. As the measurements themselves were taken over at least five bin positions, the corresponding area for the five positions was taken as the measurement signal. The statistical variation in the total counts at the peak signal in each scan is taken to define the uncertainty in the area count rate. Figure 7 shows the signal from channel 1 for the measurement at bin position 70.1 as plotted in figure 6 (the peak of scan F in table 8). The count/s in the line were 97.0 with

7374 counts obtained in 76 seconds. The full-width half-maximum of the fitted Gaussian is 7.9 bins.

Table 8. Relative intensity calibration data for channel 1

a) Measurements with the BCS

Scan	Time	y (steps)	x (mm)	Bin at peak	Counts	Count/s	Area(*)	Normalised area
A	1016	y0	54.5	103.9	7273	94.5±1.1	414.9	415
Am	1016	y0	54.5	103.9	7273	94.5±1.1	331.3	
Bm	1208	y0	54.5	103.8	6867	94.1±1.1	312.4	
C	1228	195278.5	26.0	37.4	900	90.0±3.0	375.8	397±15
Dm	1242	y0	54.5	103.8	6923	94.8±1.1	313.6	
Em	1331	y0	54.5	103.8	8480	101.0±1.1	340.4	
F	1344	199278.5	40.0	70.1	7374	97.0±1.1	368.3	359±7
Gm	1353	y0	54.5	103.8	7424	103.1±1.2	338.5	
H	1403	207278.5	69.6	139.0	7481	93.5±1.1	407.3	403±7
Im	1414	y0	54.5	103.9	8256	97.1±1.1	330.3	
J	1422	211278.5	83.0	170.0	7360	86.6±1.0	367.9	365±6
Km	1436	y0	54.5	103.8	8333	104.2±1.2	340.0	
L	1445	215278.5	97.5	203.1	7455	86.7±1.0	379.2	369±6
Mm	1500	y0	54.5	103.8	7915	101.5±1.1	341.3	

(*) The area is that under the curve in a plot of counts/s versus x position. An x position width of 3 points was used for the y monitor signal area, while the measurements themselves were over 5 positions.

b) X-ray monitor measurements

(The counts in 60 seconds are the sum of six 10 second measurements and the statistical uncertainty (root counts) is 0.54% for each 60 second total.)

Time	Counts in 60s
0947	35310
1025	34728
1120	34668
1150	34566
1245	35034
1310	35196
1320	35346
1502	35226

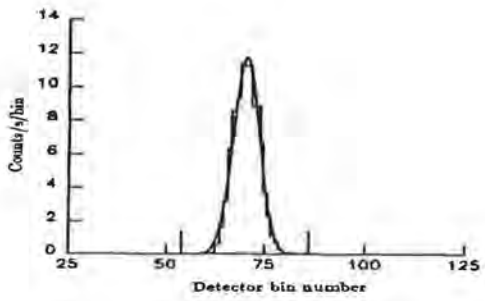

Figure 7. The channel 1 position spectrum for the measurement in figure 6 at detector bin number 70

During the measurements the x-ray direct beam monitor essentially gave a constant reading. However, the y monitor showed a variation, ranging from 312.4 to 341.3 with a mean of 331.0±11.8 counts bin/s. Since each measurement shown in table 8 was sandwiched between two y monitor measurements, a linear interpolation was used to estimate a value for the y monitor at the time of the observation. The signal observed was then normalised to the mean y monitor value, given in table 8. Although the correction has a rather large uncertainty, being the difference of two nearly equal numbers, the resulting normalised value has a relatively small uncertainty because the correction is small. In table 8 the normalised counts are assigned uncertainties relative to the mean y monitor signal. The average of the normalised sensitivity for all the measurements was taken as unity and the measurements are plotted relative to this average as a function of bin position in figure 8. The mean y monitor position is shown without error bars. This represents the relative intensity calibration since it shows the response of channel 1 at different bin positions relative to the mean y monitor signal.

7.2 Channel 2

Table 9 contains the details of the various measurements for the relative intensity calibration for channel 2. The y monitor rotation position was y0 = 202978.5 steps. The x-ray direct beam monitor signal was 9% larger at the end of the measurements than at the beginning. This monitor signal had in fact increased gradually throughout that particular day. The y monitor signal had also varied during the measurements. The results were normalised as described above for channel 1 and are given also in table 9. The resulting relative intensity calibration is plotted in figure 8.

7.3 Channel 3

Table 10 gives the results of the various measurements needed for the relative intensity calibration of channel 3. Two separate experimental runs were carried out, the first one as for channels 1 and 2 with y0 = 225150.5 steps. In the second run with y0 = 258311.5 steps, only the three points spanning the peaks of the profiles (cf. figure 6) were measured and the y monitor was not checked between the measurements at the various x positions but only at the beginning and end of the run. This second run was carried out as a cross check following an optical alignment check. For the first run, the direct beam x-ray monitor signals before and after the BCS measurements were again essentially constant while the y monitor signals showed no more than a 5% variation. For the second run both

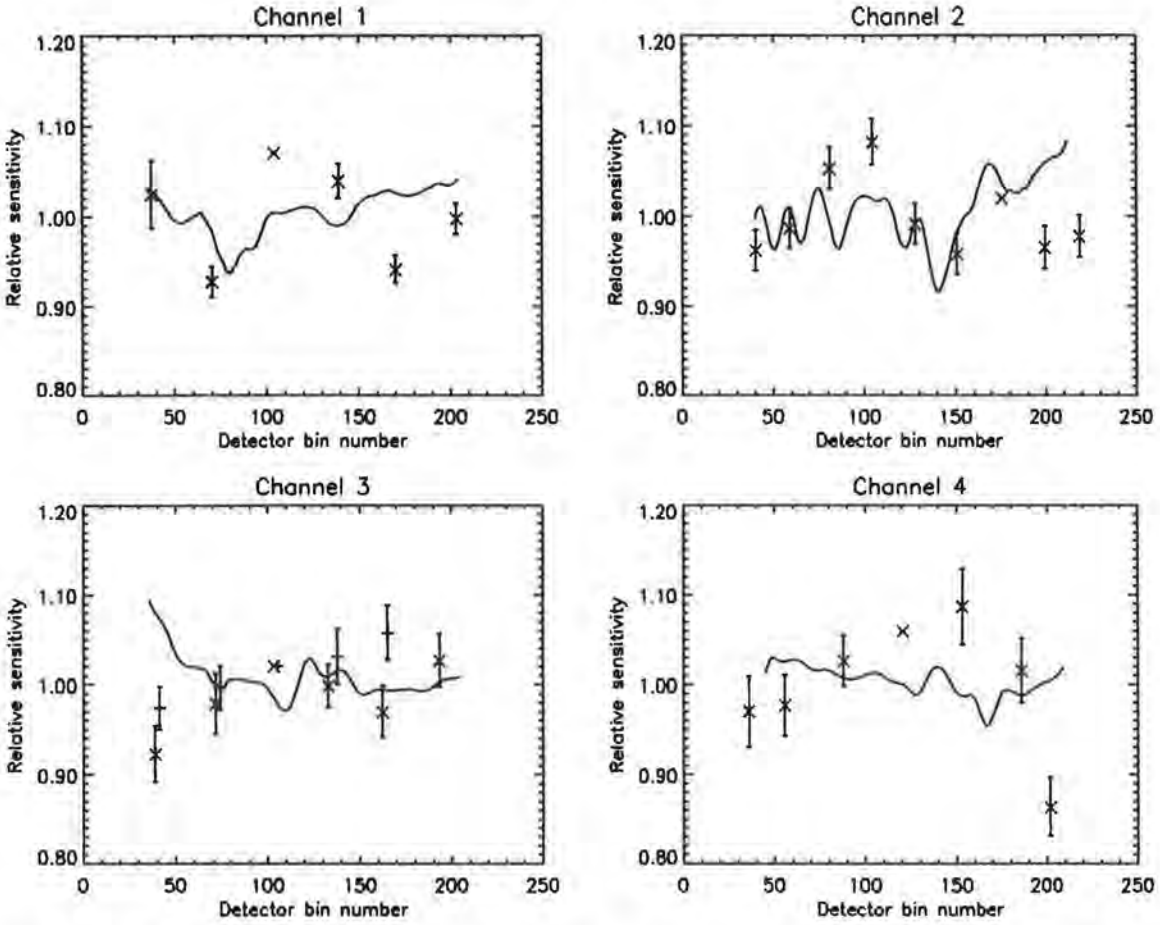

Figure 8. The relative intensity calibration for each channel. The experimental results are shown with uncertainties and the predicted responses are shown as solid lines.

x-ray and y monitors were within 2% of each other. The results for both runs were normalised as for channels 1 and 2 and are given in table 10. The relative intensity calibration data are plotted in figure 8 and each run is assigned a different symbol. There is agreement between the results of the two calibration runs within the uncertainties of the measurements, except at one position.

7.4 Channel 4

The results of the measurements for channel 4 are given in table 11 where y0 = 239389.5 steps. Again the direct beam x-ray monitor varied little and the y monitor had a range +5% and -4% about its mean value. The normalisation was carried by the method used for the other channels. The x-ray monitor signal for this channel was low, primarily because of the low efficiency of the channel-cut crystal at the wavelength of the molybdenum Lα lines. The BCS integration time was increased by 50% but still the total counts were lower than for the other channels, resulting in greater statistical uncertainties. The relative calibration for this channel is plotted in figure 8.

Table 9. Relative intensity calibration data for channel 2

a) Measurements with the BCS

Scan	Time	y (steps)	x (mm)	Bin at peak	Counts	Count/s	Area(*)	Normalised area
A	1020	y0	82.5	175.8	5179	58.9±0.8	431.6	450
Am	1020	y0	82.5	175.8	5179	58.9±0.8	155.1	
B	1044	206978.5	93.0	199.5	4201	56.0±0.9	414.8	426±10
Cm	1058	y0	82.5	175.7	4450	60.1±0.9	158.6	
D	1114	209978.5	101.5	218.7	5995	56.0±0.7	414.4	431±10
Em	1128	y0	82.5	175.9	4957	55.7±0.8	152.3	
F	1145	179978.5	24.0	40.2	4487	54.7±0.8	407.1	425±10
Gm	1202	y0	82.5	176.0	4438	58.4±0.9	157.8	
H	1219	182978.5	32.0	58.9	4897	58.3±0.8	440.0	435±10
Im	1233	y0	82.5	176.0	4902	61.3±0.9	170.6	
J	1248	186978.5	41.5	81.0	5230	62.3±0.9	459.2	464±10
Km	1306	y0	82.5	176.0	4341	60.3±0.9	146.9	
L	1321	190978.5	51.5	104.4	5074	60.4±0.9	458.8	477±11
Mm	1334	y0	82.5	176.1	4455	61.0±0.9	162.7	
N	1347	194978.5	61.5	127.8	4769	60.4±0.9	450.3	438±10
Om	1401	y0	82.5	176.1	4499	61.6±0.9	169.9	
P	1414	198978.5	71.5	150.7	5125	58.9±0.8	442.0	423±10
Qm	1425	y0	82.0	174.4	4818	64.2±0.9	168.3	

(*) The area is that under the curve in a plot of counts/s versus x position. An x position width of 3 points was used for the y monitor signal area, while the measurements themselves were over 8 positions.

b) X-ray monitor measurements

(The counts in 60 seconds are the sum of six 10 second measurements and the statistical uncertainty (root counts) is 0.56% for each 60 second total.)

Time	Counts in 60s
1003	31692
1432	34578

Table 10. Relative intensity calibration data for channel 3

1) First run

1a) Measurements with the BCS

Scan	Time	y (steps)	x (mm)	Bin at peak	Counts	Count/s	Area(*)	Normalised area
A	1312	y0	64.5	101.9	3558	47.4±0.8	360.2	363
Am	1312	y0	64.5	101.9	3558	47.4±0.8	112.7	
B	1409	228250.5	77.5	71.5	4226	45.9±0.7	352.4	348±12
Cm	1420	y0	64.0	103.1	3454	47.3±0.8	115.4	
D	1427	231250.5	91.5	38.9	3965	47.2±0.8	332.4	328±11
Em	1501	y0	64.5	101.9	3444	47.3±0.8	113.2	
F	1506	216250.5	26.0	193.2	3652	46.6±0.8	363.6	365±11
Gm	1537	y0	64.0	103.2	3548	46.4±0.8	112.7	
H	1547	219250.5	39.0	162.3	4075	49.1±0.8	345.2	345±10
Im	1614	y0	64.0	103.1	4067	47.8±0.8	116.3	
J	1621	222250.5	51.5	132.9	3617	48.5±0.8	360.5	355±10
Km	1649	y0	64.0	103.1	3351	45.3±0.8	111.6	

(*) The area is that under the curve in a plot of counts/s versus x position. An x position width of 3 points was used for the y monitor signal area, while the measurements themselves were over 7 positions.

1b) X-ray monitor measurements

(The counts in 60 seconds are the sum of six 10 second measurements and the statistical uncertainty (root counts) is 0.60% for each 60 second total.)

Time	Counts in 60s
1224	27444
1303	27408
1653	27828

Table 10. continued

2) Second Run

2a) Measurements with the BCS

Scan	Time	y (steps)	x (mm)	Bin at peak	Counts	Count/s	Area(*)	Normalised area
A	1011	y0	63.0	105.8	3601	45.0±0.8	161.2	164
B	1031	261311.5	76.5	74.0	3328	46.2±0.8	158.6	160±4
C	1035	264311.5	90.0	41.3	3777	44.4±0.7	156.1	156±4
E	1106	252311.5	8.0	165.0	3601	49.3±0.8	170.7	170±5
F	1119	255311.5	49.5	137.8	3473	47.6±0.8	166.5	165±5
G	1127	y0	63.5	104.5	3784	45.6±0.7	166.1	

(*) The area is that under the curve in a plot of counts/s versus x position. An x position width of 4 points was used for the area measurements.

2b) X-ray monitor measurements

(The counts in 60 seconds are the sum of six 10 second measurements and the statistical uncertainty (root counts) is 0.61% for each 60 second total.)

Time	Counts in 60s
0936	27036
0953	26700
1136	27378

7.5 The effect of the detector window on the relative calibration

The uniformity of the detector beryllium window can affect the uniformity of the relative calibration. Although it was not possible to make measurements using the flight windows, the transmissions of the flight spare windows were measured using molybdenum Lα radiation. A description of the tests and their results is given in Appendix C. It was estimated that the thickness of the two windows was 124±4 and 129±4 microns, while the nominal thickness was quoted as 125 microns. This gives average transmissions for channels 1,2 3 and 4 of 97%, 97%, 83% and 46% respectively. Hence variations in the window thickness can only really affect the response of spectrometer BCS-B. Noting the variation in transmission as measured using molybdenum Lα radiation and changing this to a variation in transmission at the wavelengths of channels 3 and 4 shows that if the worst variability in thicknesses applied to flight windows then the transmission for channels 3 and 4 would have the range (83±1)% and (46±5)% respectively. This could contribute ± 1% and ±10% to the uniformity of response for channel 3 and 4 respectively.

Table 11. Relative intensity calibration data for channel 4

a) Measurements with the BCS

Scan	Time	y (steps)	x (mm)	Bin at peak	Counts	Count/s	Area(*)	Normalised area
A	1653	y0	68.0	120.6	2372	22.8±0.5	249.6	243
Am	1653	y0	68.0	120.6	2372	22.8±0.5	122.6	
B	1736	245389.5	82.0	87.9	2687	24.2±0.5	241.8	236±7
Cm	1759	y0	68.0	120.4	2729	24.8±0.5	122.4	
D	1804	251389.5	96.0	55.7	2578	23.7±0.5	227.8	224±8
Em	1828	y0	68.0	120.4	2434	23.0±0.5	116.4	
F	1850	255389.5	105.0	35.8	2428	22.9±0.5	217.0	223±9
Gm	1900	y0	68.0	120.3	2558	22.8±0.5	115.3	
H	1921	233389.5	54.0	153.1	2544	24.5±0.5	247.0	250±10
Im	1933	y0	68.0	120.2	2559	23.9±0.5	19.9	
J	1940	227389.5	40.0	185.6	2383	22.5±0.5	231.3	233±8
Km	2002	y0	68.0	20.4	2556	23.9±0.5	113.8	
L	2026	224389.5	33.0	201.8	2420	22.6±0.5	202.1	198±7
Mm	2038	y0	68.0	120.5	2522	24.0±0.5	125.7	

(*) The area is that under the curve in a plot of counts/s versus x position. An x position width of 3 points was used for the y monitor signal area, while the measurements themselves were over 6 positions.

b) X-ray monitor measurements

(The counts in 60 seconds are the sum of six 10 second measurements and the statistical uncertainty (root counts) is 0.70% for each 60 second total.)

Time	Counts in 60s
1450	20922
1727	20394
2057	20460

7.6 The comparison of measurements and a model of the predicted response

Appendix A contains a description of the modelling of the relative response of each spectrometer as a function of bin position on the detector. This model includes the results of various tests carried out on components of the BCS, but not necessarily flight components. Using the data from Appendix A, the boxcar (running) average of the relative response was obtained, averaging over nine bins at a time. Averaging over seven, nine or eleven bins made no appreciable difference to the result. The range of values chosen easily encompasses the range of the full-width half-maximum bin widths of the x-ray beams measured for any of the channels (as shown in figure 7 for channel 1). Note that in the calculation described in Appendix A the predicted response in the central 129 bins has been normalised to unity (cf. the normalisation of the experimental measurements). As shown in figure 8 there is very good agreement between the measurements and predictions, although the result for bin 202 in channel 4 appears rather low. The relative sensitivity for each channel can be taken to be uniform to ±10%.

8. The absolute intensity calibration

The spectrometer measurements yielding the intensity calibration are the scans in angle at a fixed position of the spectrometer. Thus the Bragg angle of the incident radiation is changed yet the portion of the crystal/detector combination illuminated remains the same. In the idealised case of a parallel monochromatic beam incident on a flat crystal which is rotated and when a detector is used to measure both the reflected beam and the incident beam at each position, the integrated reflectivity of the crystal can be derived. However, in the present case the incident beam is divergent and not monochromatic. Burek et al. (1974) and Evans and Leigh (1976) have shown experimentally for a wide range of cases that, although the rocking curve shape may be distorted, the value of the integrated reflectivity measured did not change within the few percent of the experimental uncertainty. Evans and Leigh (1976) supported their measurements with a general proof. Furthermore, in the present experiment, because two separate detectors are used, the effective integrated reflectivity of the flight crystal/detector combination is obtained.

In table 12, the ratios of the integral of the signals measured in a particular channel divided by the appropriate monitor signals are given for both the feet west and feet east configurations. The uncertainties quoted are derived from considerations of the statistical uncertainties in the BCS and monitor signals. The bin for which the peak signal was obtained is also indicated. The east and west scans were done to provide insight into any problems caused by having the calibration done with the BCS crystal in say the (+1) rather than the (-1) orientation with respect to the (1,-1) channel-cut crystal. In fact, the only case where there was a noticeable difference was found in channel 2 where the feet west (1,-1,-1) scan was lower in relative peak height (19%) and had a larger full-width half-maximum than the feet east scan. However, after integration the ratio of the feet west result to the feet east result is 1.08. For channel 3 only the feet west scan for the stronger Kα line was done and unfortunately this was later found to have a problem with the x-ray

set beam intensity and had to be discarded. For channel 4 where results were obtained for the case without shims and the two cases with shims, the results for the flight configuration are given in table 12.

Table 12. Measurements of effective integrated reflectivities

X-ray line	Co Kα (1.789Å)	Ho Lα (1.845Å)	Ca Kβ (3.090Å)	Mo Lα (5.407Å)
Integrated BCS signal/monitor (arc s)				
feet west	17.3±0.7	21.7±1.3	19.8±1.6	24.3±1.8
feet east	17.5±0.7	20.2±1.2	19.1±1.5	24.4±1.8
average	17.4±0.7	21.0±1.6	19.4±1.6	24.3±1.8
bin (west, east)	104, 96	176, 177	136, 125	125, 131
Average of west and east linear scans (arc s)	16.4±1.7	21.5±2.6	17.2±1.4	25.1±2.5
Effective integrated reflectivity (μR)	52.1±3.4	67.3±6.7	106.4±9.9	76.0±7.9
Theoretical crystal integ. reflectivity (μR)	65.4	66.9	102.0	207.3
Detector factor	0.82×0.96 (±4%)	0.81×0.96 (±3.6%)	0.71×0.98 (±1.7%)	0.29×1 (±3%)
Theoretical effective integ. reflectivity (μR)	51.4	52.6	71.0	60.12
Exp./Theor. effective integrated reflectivity	1.01±0.08	1.28±0.13	1.50±0.14	1.26±0.14

Since the spectrometers have bent crystals, the scans where the angle of the spectrometer relative to the beam was kept fixed and the spectrometer moved in the x-ray beam (as in the relative intensity calibration) should yield the same result as the scans where the position is fixed and the Bragg angle changed. Such fixed angle scans did not extend far enough into the wings of the profile. However, extrapolating the profiles slightly, integrating, allowing for the x-ray monitor signals and using the gradients given in tables 5 and 6 to convert from bins to arc seconds gives the results shown in table 12 for the average of the feet west and east scans. The results from the different scan techniques agree within the uncertainties of the measurements and are at worst 11% different.

Although the measurements using either BCS were taken relative to the x-ray monitor, in deriving the absolute intensity calibration the counts/s observed by the monitor must be converted to photons/s by allowing for the transmission of the x-ray monitor detector window and the absorption of its filling gas. The transmission of the x-ray monitor detector window was not measured by the manufacturers of the detector. The theoretical transmission of the window (6 microns of mylar) is given in table 3. The uncertainties quoted were deduced noting that for channels 1 and 2 changing the thickness by a factor of two makes less than 1% difference to the transmission and for channels 3 and 4 changing the thickness of the mylar by 1 micron changes the transmission by 1% and 4.2%, respectively. The gas efficiencies given in table 3 were calculated by Trow (1992)

and their uncertainties estimated assuming the photoabsorption cross-section of the counter gas is known to ±5%.

The signals measured by both the monitor and spectrometers must also be corrected for polarisation effects. The x-ray set emits unpolarised radiation which can be regarded as being composed of two orthogonally plane polarised components. However, both the channel-cut and the BCS crystals respond differently to radiation polarised with the electric vector in the plane of incidence (π component) and with the electric vector perpendicular to the plane of incidence (σ component). The ratio of the integrated reflectivities of the two components, $k = R_\pi/R_\sigma$, is $|\cos(2\theta)|$ for a perfect crystal with no absorption (θ is the Bragg angle, see e.g. Burek 1976). The difference in integrated reflectivity for the two components is allowed for assuming the crystals are perfect and non-absorbing. The values of k for the quartz channel-cut crystal and the BCS crystals at the wavelengths of the x-ray lines used are given in table 13. Also given are the factors by which the signals measured using the x-ray monitor and the BCS must be multiplied to correct for the polarisation differences. It is assumed that these factors introduce no additional uncertainties.

Table 13. Polarisation factors

BCS Channel	1	2	3	3	4
			K β	K α	
k (quartz crystal)	0.853	0.843	0.561	0.481	0.343
k (BCS crystal)	0.600	0.574	0.194	0.410	0.368
Monitor factor	1.158	.169	1.522	1.624	1.789
BCS factor	1.392	1.420	1.885	1.826	1.918

The effective integrated reflectivities from the measurements are given in table 12. The uncertainties quoted were derived from the uncertainties already discussed as well as uncertainties arising from the vertical alignment of the apparatus and the use of non-flight electronics. The height of the x-ray direct beam monitor window exposed to x-rays was set so that it subtended the same angle at the x-ray source as the BCS aperture. An allowance of ±3% in the uncertainties is made to allow for any small error in setting the x-ray monitor to the correct position and height. The prototype electronics (E-box) was used in place of the flight E-box for the tests described in this work. To check for any differences, tests with the motion system de-energised and the flight E-box in place were carried out. The correction was found to be negligible but the ±2% uncertainty in this result is added to the error budget.

The theoretical effective integrated reflectivities for the four channels are also presented in table 12. These were derived by taking the data of Cowan (1991) for the theoretical integrated reflectivities and multiplying by the detector factor which is taken as the

product of the window transmission and the filling gas absorption for the flight detectors. The measurements of detector window transmission are discussed in Appendix C and the gas absorption factors were supplied by Trow (1992). The ratios of the experimental and theoretical effective integrated reflectivities are also given in table 12. For channel 1 experiment and theory are in excellent agreement while for the other channels the experimental value is higher than the theoretical prediction and they do not agree within the uncertainties.

The sensitivity or effective area S (cm^2) of a bent crystal spectrometer can be derived from the expression given by Rapley et al. (1977),

$$S = T_{filt} \times A_{pr} \times T_W \times T_{det} \times R_{int} / d\theta \qquad (3)$$

where T_{filt} is the thermal filter transmission, A_{pr} is the projected area of the crystal, T_W is the detector window transmission, T_{det} is the detector gas absorption factor, R_{int} is the crystal integrated reflectivity and $d\theta$ the range of Bragg angles corresponding to the wavelength range of the channel. In table 14 the various factors needed to evaluate the sensitivity for each channel are drawn together. The transmissions of the thermal filters are taken from Appendix E, the dimensions of the crystals are taken from table 1, the factor F (the product of T_W, T_{det} and R_{int}) is the measured effective integrated reflectivity and $d\theta$ is calculated from the results in table 6. For BCS-A the factor F can be obtained from table 12 since the x-ray lines used lie within the wavelength ranges of the channels. For BCS-B this is not the case so the results given in table 12 must be scaled to allow for the wavelength change. For channels 3 and 4 the ratios of the theoretical effective integrated reflectivities at the appropriate wavelengths are used to scale the measured effective integrated reflectivities, with corresponding changes to the uncertainties. The resulting measured effective areas (S') with uncertainties are given in table 14. These effective areas were measured at the standard positions used in the wavelength and relative intensity calibrations i.e. the points shown in figure 8 without error bars. However, if the relative calibration is taken as uniform the ratio of the relative sensitivity at the standard position to the average sensitivity for the channel must be allowed for. The corresponding effective areas (S) and uncertainties are given in table 12. In the calculation of the uncertainties the standard deviation of the average of the relative sensitivities in each channel was used to allow for the spread in values of the relative sensitivity.

Table 14.

Channel	1	2	3	4
T_{filt}	0.98±0.005	0.98±0.005	0.90±0.02	0.66±0.03
A_{pr} (cm^2)	32.05±0.08	33.64±0.11	35.98±0.07	35.00±0.18
$d\theta$ (rad)	0.01464	0.01901	0.01235	0.02376
F (μrad)	52.1±3.4	67.3±6.7	117.9±11.3	77.3±9.0
S' (cm^2)	0.112±0.007	0.117±0.011	0.309±0.031	0.075±0.009
S (cm^2)	0.104±0.009	0.114±0.012	0.303±0.032	0.071±0.010

9. Conclusions

The laboratory end-to-end calibration of the BCS has been described. The wavelength calibration indicates that the desired wavelength ranges have been achieved. That the wavelength ranges are slightly larger than those required is a result of purposely bending the crystals to slightly smaller radii than desired. The relative efficiency measurements show that the relative response of each channel is uniform. For channel 1 the relative sensitivity is within 14% of that at the standard position and for the other channels is within 10% except for one measurement in channel 4. Comparisons of experimental measurements and model predictions yield good agreement. The relative response of each channel can be taken as unity to ±10%. Comparisons of measured and expected spectrometer effective integrated reflectivities show that channel 1 has the expected value while channels 2, 3 and 4 have respectively 28%, 50% and 26% greater than expected values. The measured effective areas, with uncertainties, for the flight wavelength ranges are 0.104±0.009 cm^2, 0.114±0.012 cm^2, 0.303±0.032 cm^2 and 0.071±0.010 cm^2 for channels 1 to 4 respectively when the relative response within a channel is taken to be uniform.

Acknowledgements

The authors thank J. E. Bateman, R. W. Hayes, A. Joyce, D. J. McPhail, H. S. Taylor, E. F. Towndrow and P. C. J. White for their help in the design, building and commissioning of the end-to-end test apparatus. P. L. Cowan, R. D. Deslattes, A. Henins and B. J. Kent are thanked for their advice especially pertaining to crystal physics. Members of the BCS consortium are thanked for their help and advice.

References

Bateman J. E. and Joyce A., 1990, private communication

Brennan S. and Cowan P. L., 1992, Rev. Sci. Instr., **63**, 850-853

Burek A. J., 1976, Space Science Instrumentation, **2**, 53-104

Burek A. J., Barrus D. M. and Blake R. L., 1974, Astrophys. J., **191**, 533-543

Cowan P. L., 1991, private communication

Culhane J. L., Hiei E., Doschek G. A., Cruise A. M., Ogawara Y., Uchida Y., Bentley R. D., Brown C. M., Lang J., Watanabe T., Bowles J. A., Deslattes R. D., Feldman U., Fludra A., Guttridge P. R., Henins A., Lapington J., Magraw J. E., Mariska J. T., Payne J., Phillips K. J. H., Sheather P., Slater K., Tanaka K., Towndrow E. F., Trow M. W. and Yamaguchi A., 1991, Solar Physics, **136**, 89-104

Evans K. D. and Leigh B., 1976, Space Science Instrumentation, **2**, 105-123

Fludra A., Phillips A. T. and Trow M. W., 1990, private communication

Kent B. J., 1988, private communication
Rapley C. G., Culhane J. L., Acton L. W., Catura R. C., Joki E. G. and Bakke J. C., 1977, Rev. Sci. Instrum. **48**, 1123-1130
Trow M. W., 1992, private communication

APPENDIX A

The Monte Carlo calculation of relative bin sensitivities

The end-to-end testing of the BCS spectrometers was extensive, and sampled the sensitivity of the four channels at a number of points over the spectrometer apertures. While extraordinarily complete, it was not possible to investigate details of spectrometer performance on a bin-by-bin basis. This limitation was due to the finite amount of time available for testing and to the fact that the spread of the beam of the x-ray set spanned several bins of the detector. While it might have been possible to narrow the beam to a single bin with a very long apparatus and narrow slits, this was impractical and unnecessary, as most properties of the spectrometers varied slowly over the range. Prior to assembly of the components (crystals, detectors, windows, thermal filters and structures), sufficient measurements were made to allow necessary details to be modelled by a Monte Carlo type computer calculation. These gave relative bin sensitivities that when suitably averaged could be compared with the end-to-end results and used to correct raw data.

The following measurements are available as a result of work conducted at MSSL, NIST, NRL and RAL:

(1) The direction of the local crystal normal was measured with x-rays at over 150 positions regularly spaced over the entire surface of each crystal, with 2 arc second accuracy.

(2) The positions of the detector bins and their widths were measured with 10 μm accuracy along the length of each detector window.

(3) The clear area of the detector beryllium window was measured with 1% accuracy at 0.5 mm intervals over the entire length of each window.

(4) The offset angle of each crystal was measured with x-rays.

(5) The dimensions and angles of the support structures were accurately determined.

(6) The uniformity and thickness of the beryllium windows and kapton thermal filters were carefully measured and found to be quite constant.

A constant multiplier (for a given wavelength) can account for the factors in item (6) and for the reflectivity of the perfect germanium crystals. Items (1) - (3) were found to vary on a scale comparable to the bin dimensions and are best treated by computer modelling. Items (4) and (5) were necessary information for the calculations.

A model was constructed wherein the sensitivity of an ideal bin was given a value of 1.0, and the computed sensitivity for all bins tabulated. An ideal bin was taken to have the average sensitivity of the central half of the BCS detector area. This normalisation was done to avoid the ends of the crystals, detectors, and windows where their performance is irregular. The central zone of the detector is the portion of the instrument best represented by ideal values of crystal reflectivity, window transmittance and detector sensitivity, facilitating the conversion of relative sensitivities to absolute sensitivities. In this model all detectors were taken as being 256 bins wide, as was the case in the end-to-end test operations.

The Monte-Carlo process used is a ray tracing calculation wherein a large number of rays enter the BCS aperture and are traced from the crystal to the detector. The source of the rays is chosen to simulate a uniform flat continuum of x-rays coming from infinity and propagating parallel to the spectrometer -Z axis. The local crystal curvature (from NIST) is entered as tabular data and an interpolation subroutine used to provide the local normal to the crystal planes wherever a ray intersects the crystal. Similarly, the detector window area (from MSSL) is entered as a table and interpolation used to evaluate the window area over each bin. The detector bin positions form a third table (from MSSL) in which is found the starting point of each bin as a function of distance along the detector. A subroutine was written that returned a bin number when given the distance s where a ray strikes the detector.

In the calculation the Z co-ordinate is taken to be the sun-ward direction and each BCS is oriented standing on its feet with the Y axis in the upward direction as shown in figure A1. X-rays propagate in the -Z direction initially. Table A1 summarises the geometric parameters used in the calculation. In that table R, the crystal radius of curvature, was obtained by fitting the NIST measurements of curvature for the central ~2/3 of the crystal to the equation of a circle by least squares. Yl, Ys, etc., in table A1 (and indicated in figure A1), are the long and short wavelength ends of the crystals and detector, as used in the ray trace. Xofset is the offset of the crystal planes from the crystal surface. Sofset is an empirical rotation of the entire spectrometer assembly that gave the best agreement with the bin positions of the x-rays observed in the end-to-end tests. As such it is an accumulation of all the residual errors in building the spectrometers, manufacture of the crystals, the end-to-end facility and experimental errors occurring during the calibration. Further such errors are possible in the final orbital configuration due to installation of the spectrometers on the spacecraft centre panel, movement of the centre panel, final shake test, launch vibrations and changes due to zero gravity conditions.

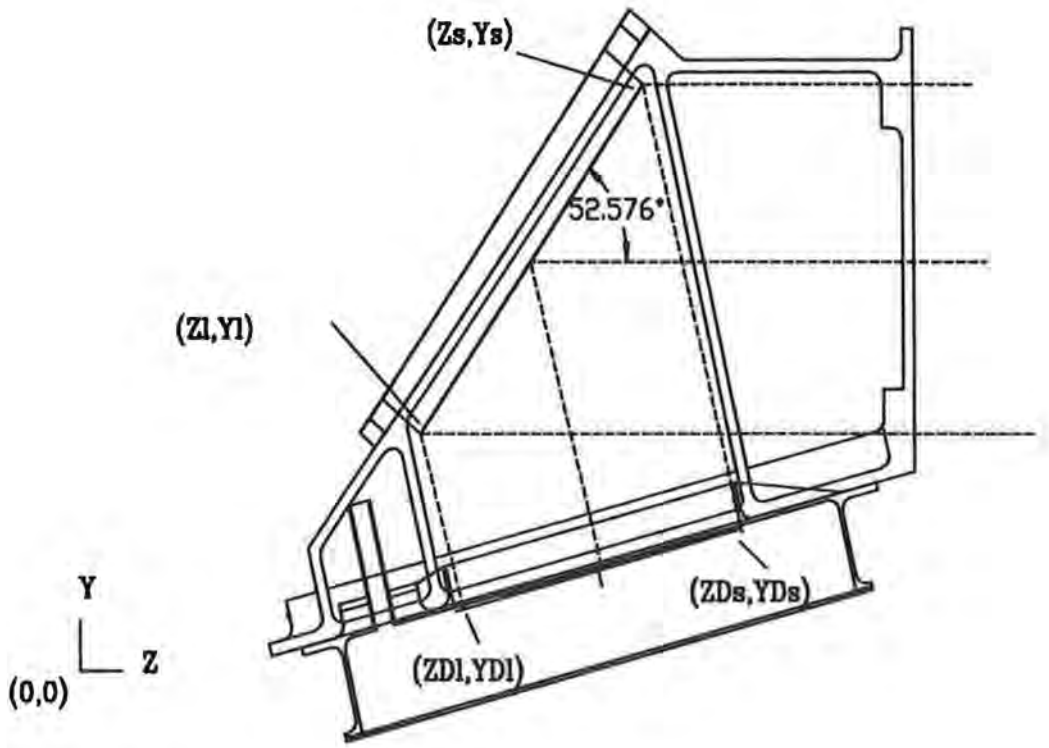

Figure A1. Schematic of BCS-B showing the axes and reference points for the calculation.

Table A1. Geometric parameters for modelling.

Channel	1	2	3	4
Ion	Fe XXVI	Fe XXV	Ca XIX	S XV
R (fitted, mm)	13640.	9450.	9120.	4650.
Ge plane	220	220	220	111
2d (A)	4.000	4.000	4.000	6.532
Yl (crystal, mm)	108.820	107.447	60.609	62.504
Zl "	83.827	84.737	103.337	101.387
Ys "	188.834	190.884	150.110	150.376
Zs "	244.367	243.540	171.825	172.999
YDl (detector, mm)	89.059	89.059	14.991	14.991
ZDl "	63.473	63.473	113.698	113.698
YDs "	36.455	36.455	36.038	36.038
ZDs "	136.495	136.495	201.252	201.252
xofset (arc second)	-102.8	136.7	-148.6	81.9
sofset "	-83.5	-161.4	314.0	-40.7

The calculation can be outlined as follows:

(1) A value of Y is selected for an incoming ray. These values are evenly spaced between Y_{min} and Y_{max} which are defined by the lower and upper ends of the crystal.

(2) The position (Y, Z) is computed where this ray intersects the crystal surface.

(3) A co-ordinate X (not perpendicular to Y & Z) is computed that gives the distance of (Y, Z) from the crystal centre, measured along an axis tangential to the crystal at its centre. (See Appendix B.)

(4) The crystal normal direction at (Y, Z) is interpolated from the NIST tables using the co-ordinate X.

(5) The incoming ray is mirrored in this normal vector and propagated until it intersects the detector. A wavelength λ for the ray is calculated using Bragg's law and the local angle of incidence at (Y, Z).

(6) The distance s from the ray intersection point to the end of the detector is calculated.

(7) The bin number corresponding to s is calculated by the subroutine using MSSL's bin position tables.

(8) A counter, n(bin), is incremented by 1, a sum, $\Sigma\lambda$ (bin) is incremented by λ and a sum $\Sigma\lambda^2$ (bin) is incremented by λ^2 .

It should be noted that the NIST measurements of crystal curvature comprised three passes along the length of each crystal, one on centre, one ~1 cm above centre and one ~1 cm below centre, see Appendix B. Rather than average the three values for each position on the crystal, steps 1 - 8 above were done three times, for each of the three curvature tables provided, with a large number (100,000) of rays , once for each crystal, to give a total of 300,000 rays.

The bin statistics were then calculated. A normalisation factor n* was computed by averaging the number of counts in bins 64 - 192 for each channel and the normalised counts per bin, int(bin) = n(bin)/n*, calculated. Likewise, an average wavelength seen by the bin was λ(bin) = $\Sigma\lambda$(bin)/n(bin) and a measure of the variance of the wavelengths falling into the bin was calculated using $\Sigma\lambda^2$. The quantity int(bin) was then multiplied by T(bin) where $0 < T \leq 1$ is the interpolated window area over the bin at the average position of the bin, again normalised to the average of the central 129 bins. The average wavelength λ(bin) was divided by 2d to get sinθ for the bin. Sinθ was thought to be of more general utility since it allows users to vary the 2d spacing as a function of crystal temperature, or to use their own preferred value.

Two tables of 256 values are provided in the BCS software for each channel, the first having the values of the relative sensitivity of each bin as calculated above. The counts seen by an ideal detector with uniform sensitivity, uniform window area and uniform bin size can be determined by dividing the observed counts(bin) by this value for each bin. The second table contains 256 values of $\sin\theta$, which when multiplied by the user's value of 2d gives λ for the bin. A corrected spectrum is then a plot of the modified counts(bin) versus λ(bin). The user should be aware that the data points are not exactly evenly spaced in λ because the bins do not have exactly the same size or spacing over the detector. The correct value of "intensity per unit wavelength" is the derivative of the above plot.

Figures A2 - A5 summarise the input and output data for the calculation for channels 1 - 4, respectively. The upper left panel is the window area as corrected for the excess weld material, the upper right panel is the bin width, the lower left is the normalised sensitivity and the lower right is $\sin\theta$, all plotted as a function of bin number. The sensitivity of the bins is most affected by the bin width, secondly by the window factor and least by crystal curvature, except perhaps at the very ends of the crystals. The values of $\sin\theta$ form a nearly linear plot, again except for the ends of the crystal. Those who only require wavelength accuracies of ±0.2 mA can use simple linear dispersion curves; likewise those who require intensities to accuracies of ± 10% or so can assume uniform sensitivity.

As these tables have been constructed for the nominal angles for each crystal, the user must correct for offsets due to flare location, spacecraft pointing and any spectrometer misalignment. The wavelength for each bin must be shifted by

$$\delta\lambda = 2d\cos\theta\delta\theta$$

where $\delta\theta$ is the total of the angle offsets, usually best determined by comparing the raw wavelengths of good lines observed in the late phase of a flare with the known laboratory wavelengths for the transitions involved. The bin sensitivities need no adjustment since a 15 arc minute angular offset only shifts the projection of the crystal on the detector by about 1 bin and it has been found that the variations due to local variations in the crystal curvature are small and relatively slowly varying.

We conclude that the bin sensitivities are mainly functions of bin width and window transmission, quantities that do not translate on the detector when the flare position moves.

Tables A2 reports the results of the calculations for each spectrometer by bin number. Tabulated are the window area factor, T(bin), the bin width in mm, the normalised sensitivity int*(bin) and the sine of the Bragg angle corresponding to the average wavelength seen in the bin.

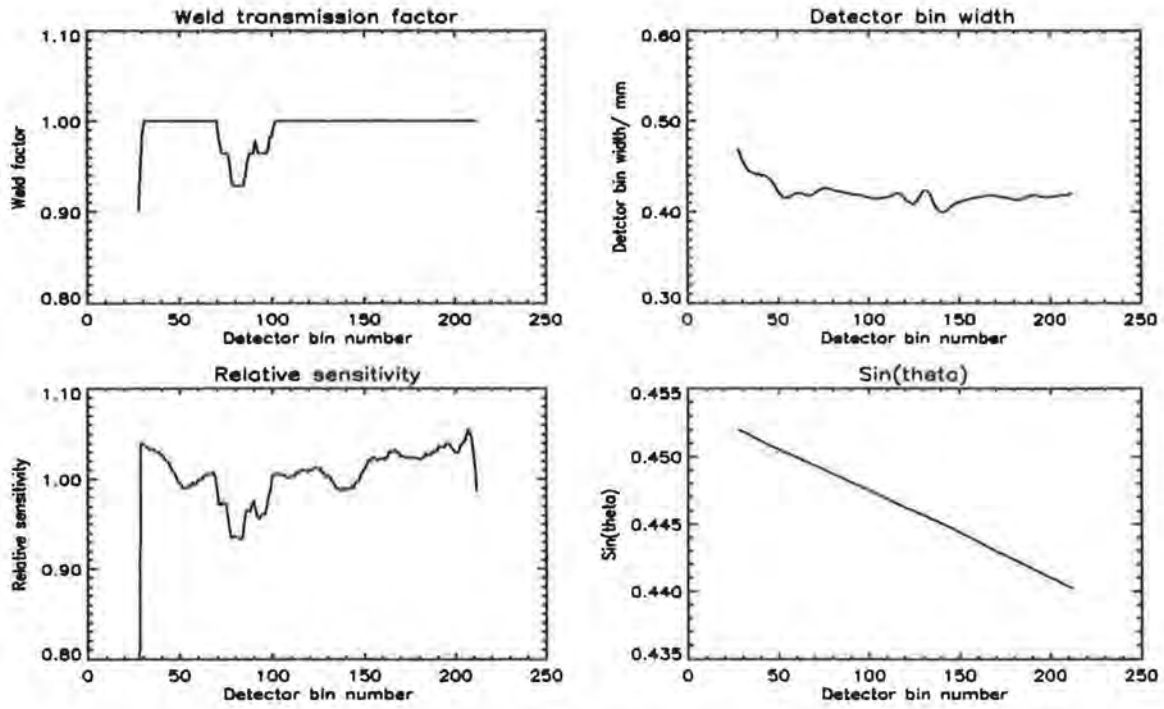

Figure A2. Input and output data graphed versus bin number for the calculations for channel 1.

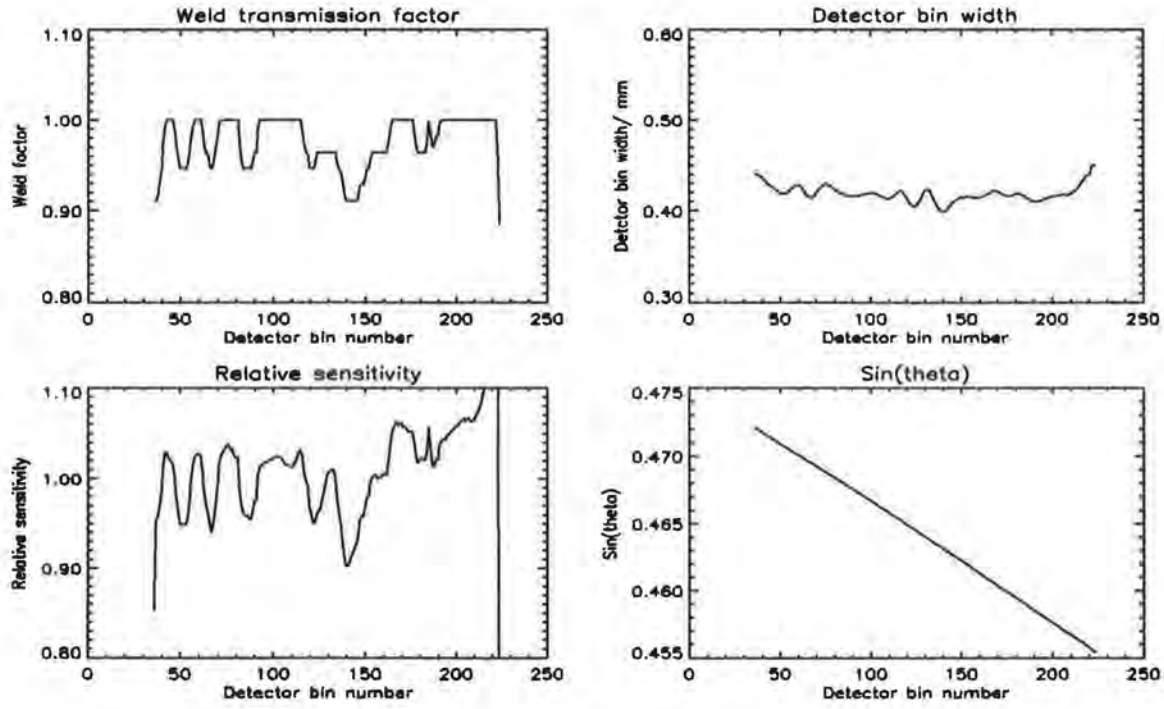

Figure A3. Input and output data graphed versus bin number for the calculations for channel 2.

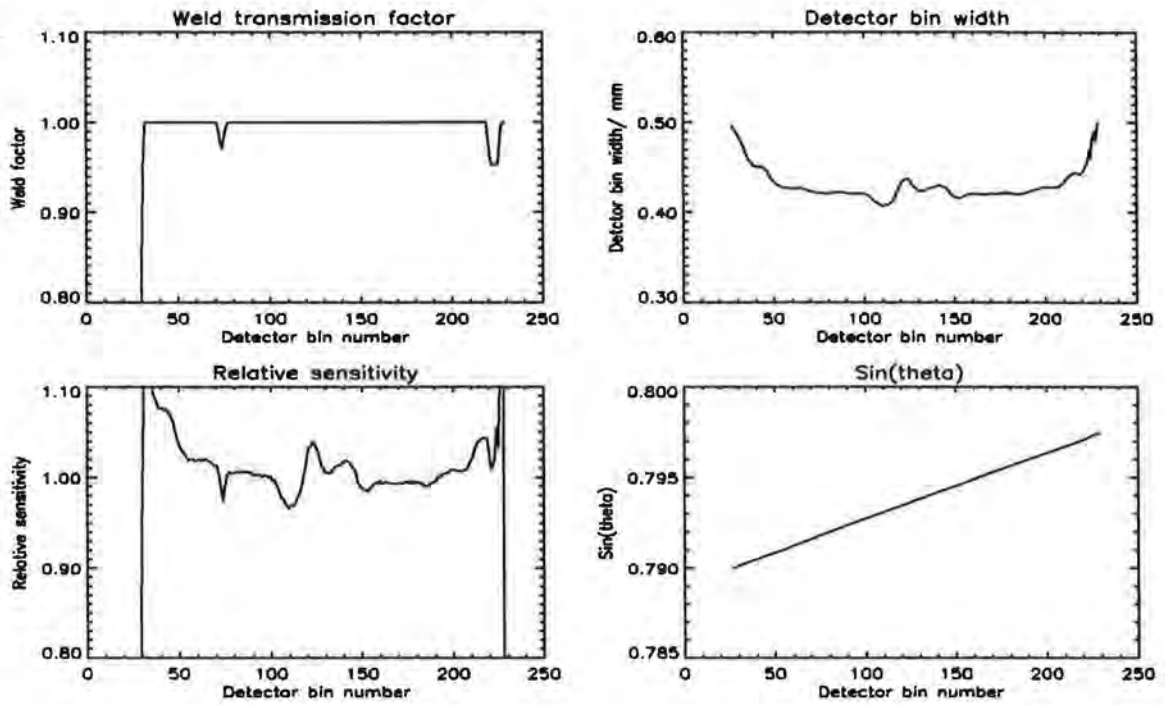

Figure A4. Input and output data graphed versus bin number for the calculations for channel 3.

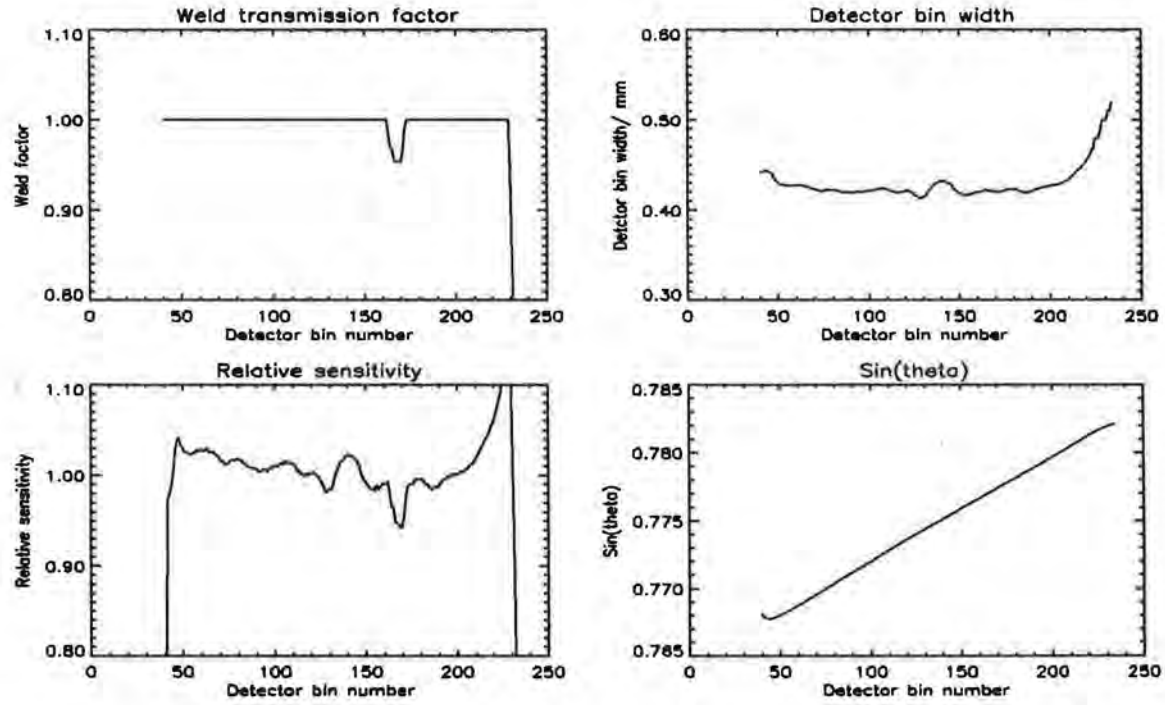

Figure A5. Input and output data graphed versus bin number for the calculations for channel 4.

Table A2. Spectrometer calibration data. For the range of bins accessible to on-axis radiation, the weld factors, the bin widths, the predicted relative sensitivity and the values of sinθ are given.

a) Spectrometer BCS-A

Channel 1					Channel 2				
Bin no.	Weld factor	Bin width (mm)	Rel. Sens.	Sinθ	Bin no.	Weld factor	Bin width (mm)	Rel. Sens.	Sinθ
28	0.902	0.4700	0.681	0.4519	36	0.911	0.4410	0.852	0.4721
29	0.949	0.4650	1.041	0.4519	37	0.911	0.4400	0.954	0.4720
30	0.987	0.4580	1.039	0.4518	38	0.916	0.4390	0.959	0.4719
31	1.000	0.4540	1.037	0.4518	39	0.931	0.4370	0.971	0.4719
32	1.000	0.4500	1.036	0.4517	40	0.946	0.4370	0.986	0.4718
33	1.000	0.4470	1.033	0.4517	41	0.975	0.4340	1.010	0.4717
34	1.000	0.4440	1.033	0.4516	42	0.994	0.4330	1.029	0.4716
35	1.000	0.4440	1.033	0.4515	43	1.000	0.4310	1.029	0.4715
36	1.000	0.4420	1.033	0.4514	44	1.000	0.4280	1.022	0.4714
37	1.000	0.4430	1.030	0.4514	45	1.000	0.4270	1.020	0.4713
38	1.000	0.4410	1.031	0.4513	46	1.000	0.4250	1.017	0.4712
39	1.000	0.4420	1.029	0.4512	47	0.987	0.4240	1.002	0.4712
40	1.000	0.4410	1.026	0.4512	48	0.973	0.4220	0.982	0.4711
41	1.000	0.4400	1.026	0.4511	49	0.959	0.4210	0.965	0.4710
42	1.000	0.4400	1.022	0.4510	50	0.946	0.4190	0.949	0.4709
43	1.000	0.4390	1.020	0.4510	51	0.946	0.4190	0.950	0.4708
44	1.000	0.4380	1.019	0.4509	52	0.946	0.4190	0.949	0.4707
45	1.000	0.4360	1.015	0.4508	53	0.946	0.4190	0.949	0.4707
46	1.000	0.4350	1.010	0.4508	54	0.952	0.4200	0.956	0.4706
47	1.000	0.4320	1.007	0.4507	55	0.966	0.4210	0.975	0.4705
48	1.000	0.4300	1.005	0.4506	56	0.980	0.4240	0.996	0.4704
49	1.000	0.4260	0.999	0.4506	57	0.995	0.4250	1.014	0.4703
50	1.000	0.4230	0.995	0.4505	58	1.000	0.4270	1.025	0.4702
51	1.000	0.4190	0.993	0.4505	59	1.000	0.4280	1.027	0.4702
52	1.000	0.4180	0.990	0.4504	60	1.000	0.4280	1.028	0.4701
53	1.000	0.4150	0.991	0.4503	61	1.000	0.4270	1.026	0.4700
54	1.000	0.4160	0.990	0.4503	62	0.987	0.4250	1.008	0.4699
55	1.000	0.4150	0.993	0.4502	63	0.972	0.4230	0.987	0.4698
56	1.000	0.4150	0.991	0.4502	64	0.964	0.4200	0.973	0.4697
57	1.000	0.4180	0.997	0.4501	65	0.962	0.4160	0.962	0.4697
58	1.000	0.4180	0.994	0.4500	66	0.947	0.4160	0.949	0.4696
59	1.000	0.4200	0.996	0.4500	67	0.946	0.4140	0.941	0.4695
60	1.000	0.4200	1.000	0.4499	68	0.956	0.4150	0.953	0.4694
61	1.000	0.4200	1.000	0.4499	69	0.970	0.4160	0.972	0.4693
62	1.000	0.4210	1.000	0.4498	70	0.984	0.4190	0.994	0.4693

63	1.000	0.4200	1.003	0.4497	71	0.998	0.4220	1.016	0.4692
64	1.000	0.4190	1.006	0.4497	72	1.000	0.4250	1.024	0.4691
65	1.000	0.4180	1.005	0.4496	73	1.000	0.4270	1.030	0.4690
66	1.000	0.4190	1.006	0.4496	74	1.000	0.4280	1.034	0.4689
67	1.000	0.4180	1.005	0.4495	75	1.000	0.4300	1.037	0.4688
68	1.000	0.4180	1.009	0.4494	76	1.000	0.4290	1.037	0.4688
69	1.000	0.4190	1.002	0.4494	77	1.000	0.4280	1.034	0.4687
70	1.000	0.4210	0.987	0.4493	78	1.000	0.4270	1.033	0.4686
71	0.988	0.4210	0.974	0.4493	79	1.000	0.4250	1.027	0.4685
72	0.973	0.4240	0.971	0.4492	80	1.000	0.4230	1.023	0.4684
73	0.964	0.4240	0.975	0.4491	81	1.000	0.4230	1.024	0.4683
74	0.964	0.4250	0.972	0.4491	82	0.971	0.4200	0.987	0.4683
75	0.964	0.4260	0.972	0.4490	83	0.953	0.4200	0.969	0.4682
76	0.964	0.4260	0.956	0.4490	84	0.946	0.4190	0.960	0.4681
77	0.955	0.4260	0.940	0.4489	85	0.946	0.4180	0.959	0.4680
78	0.940	0.4250	0.934	0.4488	86	0.946	0.4180	0.960	0.4679
79	0.929	0.4250	0.937	0.4488	87	0.946	0.4170	0.957	0.4678
80	0.929	0.4240	0.936	0.4487	88	0.946	0.4160	0.954	0.4677
81	0.929	0.4230	0.935	0.4487	89	0.953	0.4160	0.962	0.4677
82	0.929	0.4230	0.934	0.4486	90	0.964	0.4160	0.974	0.4676
83	0.929	0.4220	0.934	0.4485	91	0.964	0.4170	0.978	0.4675
84	0.929	0.4220	0.938	0.4485	92	0.991	0.4160	1.003	0.4674
85	0.929	0.4220	0.952	0.4484	93	1.000	0.4170	1.014	0.4673
86	0.942	0.4210	0.965	0.4483	94	1.000	0.4170	1.015	0.4672
87	0.957	0.4200	0.965	0.4483	95	1.000	0.4180	1.018	0.4672
88	0.964	0.4210	0.964	0.4482	96	1.000	0.4180	1.019	0.4671
89	0.964	0.4200	0.971	0.4482	97	1.000	0.4180	1.019	0.4670
90	0.964	0.4200	0.976	0.4481	98	1.000	0.4190	1.021	0.4669
91	0.978	0.4190	0.965	0.4480	99	1.000	0.4190	1.021	0.4668
92	0.972	0.4190	0.958	0.4480	100	1.000	0.4190	1.022	0.4667
93	0.964	0.4190	0.956	0.4479	101	1.000	0.4200	1.025	0.4666
94	0.964	0.4190	0.961	0.4479	102	1.000	0.4190	1.024	0.4665
95	0.964	0.4180	0.961	0.4478	103	1.000	0.4190	1.024	0.4665
96	0.964	0.4180	0.960	0.4477	104	1.000	0.4180	1.022	0.4664
97	0.964	0.4180	0.972	0.4477	105	1.000	0.4170	1.021	0.4663
98	0.970	0.4170	0.982	0.4476	106	1.000	0.4160	1.019	0.4662
99	0.982	0.4160	0.987	0.4476	107	1.000	0.4150	1.016	0.4661
100	0.982	0.4160	1.005	0.4475	108	1.000	0.4140	1.015	0.4660
101	0.995	0.4150	1.006	0.4474	109	1.000	0.4130	1.013	0.4659
102	1.000	0.4150	1.006	0.4474	110	1.000	0.4130	1.013	0.4658
103	1.000	0.4150	1.006	0.4473	111	1.000	0.4140	1.015	0.4658
104	1.000	0.4140	1.005	0.4472	112	1.000	0.4150	1.019	0.4657
105	1.000	0.4150	1.005	0.4472	113	1.000	0.4160	1.021	0.4656
106	1.000	0.4150	1.005	0.4471	114	1.000	0.4190	1.030	0.4655
107	1.000	0.4150	1.003	0.4470	115	1.000	0.4200	1.033	0.4654

108	1.000	0.4150	1.001	0.4470	116	0.986	0.4220	1.025	0.4653
109	1.000	0.4160	1.003	0.4469	117	0.972	0.4210	1.005	0.4652
110	1.000	0.4160	1.003	0.4469	118	0.964	0.4200	0.998	0.4651
111	1.000	0.4170	1.003	0.4468	119	0.961	0.4180	0.990	0.4650
112	1.000	0.4170	1.004	0.4467	120	0.947	0.4150	0.968	0.4649
113	1.000	0.4190	1.007	0.4467	121	0.946	0.4120	0.961	0.4649
114	1.000	0.4190	1.006	0.4466	122	0.946	0.4080	0.951	0.4648
116	1.000	0.4200	1.009	0.4465	124	0.964	0.4040	0.961	0.4646
117	1.000	0.4200	1.010	0.4464	125	0.964	0.4050	0.964	0.4645
118	1.000	0.4190	1.009	0.4463	126	0.964	0.4070	0.969	0.4644
119	1.000	0.4180	1.008	0.4463	127	0.964	0.4100	0.977	0.4643
120	1.000	0.4160	1.011	0.4462	128	0.964	0.4130	0.986	0.4642
121	1.000	0.4130	1.010	0.4462	129	0.964	0.4180	0.997	0.4641
122	1.000	0.4110	1.011	0.4461	130	0.964	0.4220	1.007	0.4641
123	1.000	0.4100	1.013	0.4461	131	0.964	0.4230	1.009	0.4640
124	1.000	0.4080	1.012	0.4460	132	0.964	0.4230	1.010	0.4639
125	1.000	0.4090	1.010	0.4459	133	0.964	0.4220	1.009	0.4638
126	1.000	0.4110	1.013	0.4459	134	0.964	0.4190	1.004	0.4637
127	1.000	0.4120	1.007	0.4458	135	0.951	0.4140	0.977	0.4636
128	1.000	0.4160	1.008	0.4458	136	0.946	0.4090	0.962	0.4635
129	1.000	0.4190	1.003	0.4457	137	0.941	0.4050	0.947	0.4634
130	1.000	0.4220	1.005	0.4456	138	0.927	0.4010	0.925	0.4633
131	1.000	0.4240	1.002	0.4456	139	0.914	0.4000	0.909	0.4632
132	1.000	0.4230	0.999	0.4455	140	0.911	0.3990	0.902	0.4631
133	1.000	0.4220	0.997	0.4455	141	0.911	0.3990	0.903	0.4631
134	1.000	0.4200	0.994	0.4454	142	0.911	0.4010	0.909	0.4630
135	1.000	0.4160	0.990	0.4453	143	0.911	0.4030	0.915	0.4629
136	1.000	0.4110	0.989	0.4453	144	0.911	0.4060	0.921	0.4628
137	1.000	0.4060	0.988	0.4452	145	0.911	0.4090	0.927	0.4627
138	1.000	0.4030	0.991	0.4452	146	0.914	0.4100	0.934	0.4626
139	1.000	0.4000	0.988	0.4451	147	0.928	0.4120	0.954	0.4625
140	1.000	0.4000	0.990	0.4450	148	0.929	0.4130	0.957	0.4624
141	1.000	0.3990	0.990	0.4450	149	0.929	0.4140	0.957	0.4623
142	1.000	0.4000	0.989	0.4449	150	0.934	0.4150	0.968	0.4622
143	1.000	0.4010	0.993	0.4448	151	0.946	0.4140	0.979	0.4621
144	1.000	0.4030	0.990	0.4448	152	0.946	0.4150	0.982	0.4621
145	1.000	0.4050	0.996	0.4447	153	0.959	0.4160	0.997	0.4620
146	1.000	0.4070	0.997	0.4446	154	0.964	0.4150	1.002	0.4619
147	1.000	0.4080	1.000	0.4446	155	0.964	0.4150	1.004	0.4618
148	1.000	0.4090	1.005	0.4445	156	0.964	0.4150	1.004	0.4617
149	1.000	0.4100	1.008	0.4444	157	0.964	0.4140	0.999	0.4616
150	1.000	0.4100	1.013	0.4444	158	0.964	0.4150	1.002	0.4615
151	1.000	0.4120	1.015	0.4443	159	0.964	0.4140	1.002	0.4614
152	1.000	0.4120	1.021	0.4442	160	0.964	0.4150	1.005	0.4613
153	1.000	0.4130	1.019	0.4442	161	0.964	0.4150	1.005	0.4612

154	1.000	0.4130	1.024	0.4441	162	0.964	0.4150	1.004	0.4611
155	1.000	0.4140	1.023	0.4440	163	0.975	0.4170	1.018	0.4610
156	1.000	0.4140	1.023	0.4440	164	0.989	0.4180	1.038	0.4609
157	1.000	0.4150	1.021	0.4439	165	1.000	0.4190	1.052	0.4608
158	1.000	0.4150	1.022	0.4438	166	1.000	0.4200	1.058	0.4608
159	1.000	0.4160	1.022	0.4437	167	1.000	0.4220	1.063	0.4607
160	1.000	0.4160	1.024	0.4437	168	1.000	0.4210	1.059	0.4606
161	1.000	0.4170	1.021	0.4436	169	1.000	0.4220	1.062	0.4605
162	1.000	0.4170	1.024	0.4435	170	1.000	0.4210	1.061	0.4604
163	1.000	0.4170	1.025	0.4435	171	1.000	0.4200	1.057	0.4603
164	1.000	0.4180	1.031	0.4434	172	1.000	0.4190	1.056	0.4602
165	1.000	0.4180	1.029	0.4433	173	1.000	0.4180	1.054	0.4601
166	1.000	0.4180	1.031	0.4432	174	1.000	0.4170	1.051	0.4600
167	1.000	0.4180	1.033	0.4432	175	1.000	0.4170	1.052	0.4599
168	1.000	0.4180	1.029	0.4431	176	1.000	0.4160	1.050	0.4598
169	1.000	0.4180	1.028	0.4430	177	0.987	0.4170	1.041	0.4597
170	1.000	0.4180	1.025	0.4430	178	0.973	0.4170	1.025	0.4596
171	1.000	0.4170	1.026	0.4429	179	0.964	0.4180	1.018	0.4595
172	1.000	0.4170	1.024	0.4428	180	0.964	0.4190	1.022	0.4594
173	1.000	0.4170	1.024	0.4428	181	0.964	0.4190	1.022	0.4594
174	1.000	0.4160	1.023	0.4427	182	0.964	0.4180	1.021	0.4593
175	1.000	0.4160	1.024	0.4426	183	0.964	0.4190	1.022	0.4592
176	1.000	0.4150	1.023	0.4426	184	0.974	0.4170	1.030	0.4591
177	1.000	0.4150	1.023	0.4425	185	0.999	0.4170	1.057	0.4590
178	1.000	0.4150	1.023	0.4424	186	0.985	0.4140	1.034	0.4589
179	1.000	0.4140	1.023	0.4424	187	0.971	0.4130	1.013	0.4588
180	1.000	0.4130	1.022	0.4423	188	0.972	0.4120	1.015	0.4587
181	1.000	0.4130	1.022	0.4423	189	0.982	0.4100	1.023	0.4586
182	1.000	0.4130	1.024	0.4422	190	0.982	0.4100	1.021	0.4585
183	1.000	0.4140	1.025	0.4421	191	0.996	0.4100	1.038	0.4584
184	1.000	0.4130	1.029	0.4421	192	1.000	0.4100	1.041	0.4583
185	1.000	0.4150	1.026	0.4420	193	1.000	0.4110	1.045	0.4582
186	1.000	0.4150	1.026	0.4419	194	1.000	0.4110	1.043	0.4582
187	1.000	0.4170	1.030	0.4419	195	1.000	0.4130	1.049	0.4581
188	1.000	0.4170	1.029	0.4418	196	1.000	0.4130	1.049	0.4580
189	1.000	0.4180	1.031	0.4417	197	1.000	0.4140	1.053	0.4579
190	1.000	0.4180	1.031	0.4417	198	1.000	0.4140	1.053	0.4578
191	1.000	0.4190	1.037	0.4416	199	1.000	0.4150	1.056	0.4577
192	1.000	0.4180	1.036	0.4415	200	1.000	0.4160	1.059	0.4576
193	1.000	0.4180	1.036	0.4415	201	1.000	0.4160	1.059	0.4575
194	1.000	0.4170	1.035	0.4414	202	1.000	0.4170	1.062	0.4574
195	1.000	0.4170	1.039	0.4413	203	1.000	0.4170	1.065	0.4573
196	1.000	0.4170	1.039	0.4412	204	1.000	0.4180	1.067	0.4572
197	1.000	0.4160	1.038	0.4412	205	1.000	0.4170	1.063	0.4572
198	1.000	0.4170	1.034	0.4411	206	1.000	0.4180	1.067	0.4571

199	1.000	0.4160	1.033	0.4411
200	1.000	0.4170	1.030	0.4410
201	1.000	0.4170	1.029	0.4409
202	1.000	0.4170	1.031	0.4409
203	1.000	0.4180	1.039	0.4408
204	1.000	0.4170	1.039	0.4407
205	1.000	0.4180	1.042	0.4407
206	1.000	0.4190	1.046	0.4406
207	1.000	0.4180	1.055	0.4405
208	1.000	0.4180	1.053	0.4404
209	1.000	0.4190	1.046	0.4404
210	1.000	0.4180	1.029	0.4403
211	1.000	0.4200	1.011	0.4403
212	1.000	0.4200	0.988	0.4402

207	1.000	0.4180	1.067	0.4570
208	1.000	0.4170	1.063	0.4569
209	1.000	0.4180	1.065	0.4568
210	1.000	0.4180	1.065	0.4567
211	1.000	0.4200	1.073	0.4566
212	1.000	0.4200	1.071	0.4565
213	1.000	0.4230	1.079	0.4564
214	1.000	0.4250	1.084	0.4564
215	1.000	0.4270	1.095	0.4563
216	1.000	0.4310	1.105	0.4562
217	1.000	0.4340	1.112	0.4561
218	1.000	0.4350	1.116	0.4560
219	1.000	0.4390	1.131	0.4559
220	1.000	0.4400	1.143	0.4558
221	1.000	0.4390	1.143	0.4557
222	1.000	0.4500	1.159	0.4555
223	0.962	0.4500	1.097	0.4555
224	0.885	0.4500	0.713	0.4554

b) Spectrometer BCS-B

Channel 3

Bin no.	Weld factor	Bin width (mm)	Rel. Sens.	Sinθ
27	0.081	0.4970	0.071	0.7900
28	0.308	0.4930	0.354	0.7901
29	0.593	0.4900	0.709	0.7901
30	0.815	0.4860	0.962	0.7901
31	0.957	0.4820	1.115	0.7902
32	1.000	0.4790	1.144	0.7902
33	1.000	0.4740	1.130	0.7903
34	1.000	0.4690	1.119	0.7903
35	1.000	0.4640	1.107	0.7903
36	1.000	0.4590	1.094	0.7904
37	1.000	0.4560	1.088	0.7904
38	1.000	0.4540	1.083	0.7904
39	1.000	0.4510	1.077	0.7905
40	1.000	0.4510	1.077	0.7905
41	1.000	0.4510	1.076	0.7905
42	1.000	0.4500	1.075	0.7906
43	1.000	0.4510	1.077	0.7906
44	1.000	0.4490	1.073	0.7907

Channel 4

Bin no.	Weld factor	Bin width (mm)	Rel. Sens.	Sinθ
40	1.000	0.4420	0.027	0.7682
41	1.000	0.4420	0.743	0.7679
42	1.000	0.4430	0.974	0.7678
43	1.000	0.4440	0.981	0.7678
44	1.000	0.4430	0.990	0.7678
45	1.000	0.4430	1.007	0.7678
46	1.000	0.4410	1.030	0.7678
47	1.000	0.4390	1.040	0.7678
48	1.000	0.4360	1.042	0.7679
49	1.000	0.4330	1.033	0.7680
50	1.000	0.4310	1.030	0.7680
51	1.000	0.4290	1.026	0.7681
52	1.000	0.4280	1.025	0.7682
53	1.000	0.4280	1.025	0.7683
54	1.000	0.4270	1.023	0.7683
55	1.000	0.4270	1.024	0.7684
56	1.000	0.4270	1.026	0.7685
57	1.000	0.4270	1.025	0.7686

45	1.000	0.4480	1.070	0.7907	58	1.000	0.4280	1.029	0.7686
46	1.000	0.4460	1.064	0.7907	59	1.000	0.4270	1.026	0.7687
47	1.000	0.4440	1.060	0.7908	60	1.000	0.4280	1.029	0.7688
48	1.000	0.4400	1.052	0.7908	61	1.000	0.4270	1.027	0.7689
49	1.000	0.4370	1.044	0.7908	62	1.000	0.4270	1.027	0.7689
50	1.000	0.4340	1.037	0.7909	63	1.000	0.4280	1.030	0.7690
51	1.000	0.4320	1.032	0.7909	64	1.000	0.4270	1.028	0.7691
52	1.000	0.4300	1.028	0.7909	65	1.000	0.4260	1.025	0.7692
53	1.000	0.4300	1.026	0.7910	66	1.000	0.4260	1.026	0.7693
54	1.000	0.4280	1.023	0.7910	67	1.000	0.4260	1.026	0.7693
55	1.000	0.4270	1.019	0.7911	68	1.000	0.4240	1.022	0.7694
56	1.000	0.4270	1.020	0.7911	69	1.000	0.4240	1.021	0.7695
57	1.000	0.4270	1.020	0.7911	70	1.000	0.4230	1.018	0.7696
58	1.000	0.4270	1.021	0.7912	71	1.000	0.4220	1.015	0.7697
59	1.000	0.4260	1.018	0.7912	72	1.000	0.4220	1.016	0.7697
60	1.000	0.4270	1.020	0.7912	73	1.000	0.4210	1.012	0.7698
61	1.000	0.4260	1.019	0.7913	74	1.000	0.4210	1.012	0.7699
62	1.000	0.4270	1.020	0.7913	75	1.000	0.4220	1.015	0.7700
63	1.000	0.4260	1.019	0.7914	76	1.000	0.4220	1.016	0.7701
64	1.000	0.4270	1.021	0.7914	77	1.000	0.4220	1.017	0.7702
65	1.000	0.4270	1.019	0.7914	78	1.000	0.4220	1.016	0.7702
66	1.000	0.4260	1.019	0.7915	79	1.000	0.4220	1.018	0.7703
67	1.000	0.4260	1.017	0.7915	80	1.000	0.4220	1.018	0.7704
68	1.000	0.4250	1.016	0.7915	81	1.000	0.4220	1.016	0.7705
69	1.000	0.4240	1.013	0.7916	82	1.000	0.4220	1.016	0.7706
70	1.000	0.4240	1.014	0.7916	83	1.000	0.4210	1.013	0.7707
71	1.000	0.4230	1.010	0.7917	84	1.000	0.4210	1.012	0.7707
72	0.991	0.4220	1.001	0.7917	85	1.000	0.4200	1.010	0.7708
73	0.979	0.4230	0.988	0.7917	86	1.000	0.4200	1.008	0.7709
74	0.971	0.4210	0.974	0.7918	87	1.000	0.4200	1.008	0.7710
75	0.984	0.4220	0.991	0.7918	88	1.000	0.4200	1.008	0.7711
76	0.996	0.4210	1.001	0.7918	89	1.000	0.4200	1.007	0.7712
77	1.000	0.4220	1.006	0.7919	90	1.000	0.4200	1.006	0.7712
78	1.000	0.4210	1.005	0.7919	91	1.000	0.4190	1.004	0.7713
79	1.000	0.4210	1.004	0.7920	92	1.000	0.4200	1.005	0.7714
80	1.000	0.4210	1.005	0.7920	93	1.000	0.4200	1.005	0.7715
81	1.000	0.4220	1.007	0.7920	94	1.000	0.4210	1.007	0.7716
82	1.000	0.4210	1.005	0.7921	95	1.000	0.4200	1.005	0.7716
83	1.000	0.4220	1.007	0.7921	96	1.000	0.4200	1.005	0.7717
84	1.000	0.4220	1.006	0.7921	97	1.000	0.4210	1.009	0.7718
85	1.000	0.4220	1.006	0.7922	98	1.000	0.4210	1.007	0.7719
86	1.000	0.4220	1.006	0.7922	99	1.000	0.4210	1.009	0.7719
87	1.000	0.4220	1.006	0.7923	100	1.000	0.4220	1.010	0.7720
88	1.000	0.4220	1.006	0.7923	101	1.000	0.4210	1.009	0.7721
89	1.000	0.4220	1.006	0.7923	102	1.000	0.4230	1.012	0.7722

90	1.000	0.4210	1.003	0.7924	103	1.000	0.4220	1.011	0.7723
91	1.000	0.4210	1.003	0.7924	104	1.000	0.4240	1.015	0.7724
92	1.000	0.4210	1.003	0.7924	105	1.000	0.4230	1.012	0.7724
93	1.000	0.4210	1.003	0.7925	106	1.000	0.4250	1.016	0.7725
94	1.000	0.4210	1.002	0.7925	107	1.000	0.4240	1.014	0.7726
95	1.000	0.4200	1.001	0.7926	108	1.000	0.4240	1.014	0.7727
96	1.000	0.4210	1.003	0.7926	109	1.000	0.4240	1.014	0.7728
97	1.000	0.4210	1.001	0.7926	110	1.000	0.4230	1.011	0.7729
98	1.000	0.4210	1.002	0.7927	111	1.000	0.4230	1.011	0.7729
99	1.000	0.4200	1.000	0.7927	112	1.000	0.4210	1.005	0.7730
100	1.000	0.4210	1.001	0.7927	113	1.000	0.4210	1.006	0.7731
101	1.000	0.4190	0.997	0.7928	114	1.000	0.4200	1.003	0.7732
102	1.000	0.4190	0.997	0.7928	115	1.000	0.4200	1.003	0.7733
103	1.000	0.4170	0.992	0.7928	116	1.000	0.4190	0.999	0.7733
104	1.000	0.4150	0.988	0.7929	117	1.000	0.4200	1.001	0.7734
105	1.000	0.4130	0.982	0.7929	118	1.000	0.4200	1.000	0.7735
106	1.000	0.4110	0.977	0.7930	119	1.000	0.4210	1.003	0.7736
107	1.000	0.4100	0.976	0.7930	120	1.000	0.4210	1.001	0.7736
108	1.000	0.4090	0.972	0.7930	121	1.000	0.4220	1.004	0.7737
109	1.000	0.4080	0.969	0.7931	122	1.000	0.4210	1.001	0.7738
110	1.000	0.4070	0.966	0.7931	123	1.000	0.4200	0.999	0.7739
111	1.000	0.4080	0.970	0.7931	124	1.000	0.4200	0.999	0.7740
112	1.000	0.4080	0.969	0.7932	125	1.000	0.4180	0.995	0.7740
113	1.000	0.4080	0.970	0.7932	126	1.000	0.4160	0.991	0.7741
114	1.000	0.4100	0.974	0.7932	127	1.000	0.4150	0.987	0.7742
115	1.000	0.4120	0.980	0.7933	128	1.000	0.4130	0.982	0.7743
116	1.000	0.4140	0.983	0.7933	129	1.000	0.4140	0.983	0.7743
117	1.000	0.4180	0.992	0.7933	130	1.000	0.4150	0.986	0.7744
118	1.000	0.4220	1.002	0.7934	131	1.000	0.4150	0.985	0.7745
119	1.000	0.4260	1.012	0.7934	132	1.000	0.4180	0.992	0.7746
120	1.000	0.4310	1.023	0.7935	133	1.000	0.4210	0.998	0.7746
121	1.000	0.4350	1.033	0.7935	134	1.000	0.4240	1.005	0.7747
122	1.000	0.4360	1.034	0.7935	135	1.000	0.4260	1.009	0.7748
123	1.000	0.4380	1.039	0.7936	136	1.000	0.4290	1.015	0.7749
124	1.000	0.4370	1.037	0.7936	137	1.000	0.4300	1.017	0.7749
125	1.000	0.4350	1.032	0.7936	138	1.000	0.4310	1.019	0.7750
126	1.000	0.4330	1.027	0.7937	139	1.000	0.4320	1.022	0.7751
127	1.000	0.4300	1.020	0.7937	140	1.000	0.4320	1.022	0.7752
128	1.000	0.4270	1.013	0.7937	141	1.000	0.4320	1.022	0.7752
129	1.000	0.4260	1.010	0.7938	142	1.000	0.4320	1.022	0.7753
130	1.000	0.4240	1.005	0.7938	143	1.000	0.4310	1.019	0.7754
131	1.000	0.4240	1.005	0.7939	144	1.000	0.4300	1.018	0.7755
132	1.000	0.4240	1.005	0.7939	145	1.000	0.4290	1.016	0.7755
133	1.000	0.4240	1.005	0.7939	146	1.000	0.4270	1.012	0.7756
134	1.000	0.4250	1.008	0.7940	147	1.000	0.4240	1.005	0.7757

135	1.000	0.4260	1.012	0.7940
136	1.000	0.4270	1.013	0.7940
137	1.000	0.4270	1.013	0.7941
138	1.000	0.4280	1.014	0.7941
139	1.000	0.4290	1.017	0.7942
140	1.000	0.4290	1.016	0.7942
141	1.000	0.4300	1.019	0.7942
142	1.000	0.4300	1.019	0.7943
143	1.000	0.4290	1.017	0.7943
144	1.000	0.4280	1.015	0.7943
145	1.000	0.4270	1.010	0.7944
146	1.000	0.4260	1.009	0.7944
147	1.000	0.4230	1.001	0.7944
148	1.000	0.4200	0.994	0.7945
149	1.000	0.4190	0.992	0.7945
150	1.000	0.4170	0.988	0.7946
151	1.000	0.4170	0.987	0.7946
152	1.000	0.4160	0.986	0.7946
153	1.000	0.4160	0.985	0.7947
154	1.000	0.4170	0.988	0.7947
155	1.000	0.4180	0.990	0.7947
156	1.000	0.4190	0.991	0.7948
157	1.000	0.4200	0.994	0.7948
158	1.000	0.4200	0.994	0.7948
159	1.000	0.4200	0.993	0.7949
160	1.000	0.4210	0.997	0.7949
161	1.000	0.4200	0.993	0.7950
162	1.000	0.4200	0.994	0.7950
163	1.000	0.4210	0.996	0.7950
164	1.000	0.4200	0.994	0.7951
165	1.000	0.4200	0.993	0.7951
166	1.000	0.4200	0.994	0.7951
167	1.000	0.4200	0.993	0.7952
168	1.000	0.4200	0.992	0.7952
169	1.000	0.4210	0.994	0.7953
170	1.000	0.4200	0.993	0.7953
171	1.000	0.4210	0.994	0.7953
172	1.000	0.4200	0.992	0.7954
173	1.000	0.4210	0.994	0.7954
174	1.000	0.4210	0.995	0.7954
175	1.000	0.4210	0.994	0.7955
176	1.000	0.4220	0.997	0.7955
177	1.000	0.4210	0.993	0.7955
178	1.000	0.4220	0.997	0.7956
179	1.000	0.4210	0.993	0.7956
148	1.000	0.4220	0.999	0.7758
149	1.000	0.4200	0.995	0.7759
150	1.000	0.4190	0.993	0.7759
151	1.000	0.4180	0.989	0.7760
152	1.000	0.4170	0.986	0.7761
153	1.000	0.4170	0.985	0.7762
154	1.000	0.4180	0.986	0.7762
155	1.000	0.4170	0.983	0.7763
156	1.000	0.4190	0.989	0.7764
157	1.000	0.4180	0.985	0.7764
158	1.000	0.4190	0.988	0.7765
159	1.000	0.4200	0.991	0.7766
160	1.000	0.4200	0.991	0.7767
161	1.000	0.4200	0.991	0.7767
162	1.000	0.4210	0.993	0.7768
163	0.986	0.4210	0.980	0.7769
164	0.969	0.4220	0.965	0.7770
165	0.968	0.4220	0.964	0.7770
166	0.956	0.4210	0.948	0.7771
167	0.953	0.4220	0.947	0.7772
168	0.953	0.4210	0.945	0.7773
169	0.953	0.4200	0.942	0.7773
170	0.954	0.4210	0.945	0.7774
171	0.966	0.4200	0.954	0.7775
172	0.989	0.4200	0.978	0.7776
173	1.000	0.4210	0.989	0.7776
174	1.000	0.4210	0.990	0.7777
175	1.000	0.4220	0.991	0.7778
176	1.000	0.4220	0.991	0.7778
177	1.000	0.4240	0.996	0.7779
178	1.000	0.4230	0.995	0.7780
179	1.000	0.4240	0.996	0.7781
180	1.000	0.4230	0.995	0.7781
181	1.000	0.4240	0.997	0.7782
182	1.000	0.4220	0.992	0.7783
183	1.000	0.4210	0.989	0.7784
184	1.000	0.4210	0.990	0.7784
185	1.000	0.4200	0.987	0.7785
186	1.000	0.4190	0.985	0.7786
187	1.000	0.4200	0.987	0.7787
188	1.000	0.4200	0.987	0.7787
189	1.000	0.4200	0.986	0.7788
190	1.000	0.4210	0.989	0.7789
191	1.000	0.4220	0.991	0.7790
192	1.000	0.4230	0.995	0.7790

180	1.000	0.4220	0.996	0.7956
181	1.000	0.4210	0.994	0.7957
182	1.000	0.4210	0.994	0.7957
183	1.000	0.4210	0.993	0.7958
184	1.000	0.4200	0.991	0.7958
185	1.000	0.4200	0.990	0.7958
186	1.000	0.4200	0.990	0.7959
187	1.000	0.4210	0.992	0.7959
188	1.000	0.4210	0.994	0.7959
189	1.000	0.4220	0.994	0.7960
190	1.000	0.4220	0.996	0.7960
191	1.000	0.4230	0.997	0.7960
192	1.000	0.4250	1.002	0.7961
193	1.000	0.4240	1.000	0.7961
194	1.000	0.4260	1.003	0.7962
195	1.000	0.4260	1.004	0.7962
196	1.000	0.4260	1.004	0.7962
197	1.000	0.4270	1.006	0.7963
198	1.000	0.4280	1.007	0.7963
199	1.000	0.4280	1.008	0.7963
200	1.000	0.4280	1.007	0.7964
201	1.000	0.4280	1.008	0.7964
202	1.000	0.4280	1.007	0.7964
203	1.000	0.4280	1.006	0.7965
204	1.000	0.4280	1.007	0.7965
205	1.000	0.4280	1.006	0.7965
206	1.000	0.4290	1.008	0.7966
207	1.000	0.4290	1.009	0.7966
208	1.000	0.4300	1.011	0.7966
209	1.000	0.4320	1.015	0.7967
210	1.000	0.4340	1.020	0.7967
211	1.000	0.4360	1.024	0.7967
212	1.000	0.4390	1.030	0.7968
213	1.000	0.4410	1.035	0.7968
214	1.000	0.4430	1.040	0.7968
215	1.000	0.4430	1.040	0.7969
216	1.000	0.4440	1.044	0.7969
217	1.000	0.4440	1.044	0.7969
218	1.000	0.4430	1.042	0.7970
219	1.000	0.4430	1.043	0.7970
220	0.979	0.4450	1.027	0.7971
221	0.961	0.4470	1.009	0.7971
222	0.953	0.4510	1.012	0.7971
223	0.953	0.4540	1.020	0.7972
224	0.953	0.4700	1.054	0.7972

193	1.000	0.4240	0.996	0.7791
194	1.000	0.4240	0.997	0.7792
195	1.000	0.4250	0.999	0.7793
196	1.000	0.4250	0.999	0.7794
197	1.000	0.4260	1.001	0.7794
198	1.000	0.4260	1.000	0.7795
199	1.000	0.4270	1.003	0.7796
200	1.000	0.4270	1.001	0.7797
201	1.000	0.4280	1.003	0.7797
202	1.000	0.4280	1.005	0.7798
203	1.000	0.4280	1.003	0.7799
204	1.000	0.4290	1.006	0.7800
205	1.000	0.4290	1.006	0.7801
206	1.000	0.4300	1.008	0.7801
207	1.000	0.4310	1.011	0.7802
208	1.000	0.4320	1.012	0.7803
209	1.000	0.4330	1.015	0.7804
210	1.000	0.4350	1.019	0.7805
211	1.000	0.4360	1.020	0.7805
212	1.000	0.4380	1.025	0.7806
213	1.000	0.4400	1.030	0.7807
214	1.000	0.4420	1.034	0.7808
215	1.000	0.4440	1.038	0.7809
216	1.000	0.4460	1.043	0.7809
217	1.000	0.4470	1.045	0.7810
218	1.000	0.4500	1.051	0.7811
219	1.000	0.4520	1.056	0.7812
220	1.000	0.4540	1.059	0.7813
221	1.000	0.4580	1.067	0.7813
222	1.000	0.4620	1.075	0.7814
223	1.000	0.4660	1.084	0.7815
224	1.000	0.4700	1.091	0.7816
225	1.000	0.4800	1.113	0.7816
226	1.000	0.4800	1.114	0.7817
227	1.000	0.4800	1.110	0.7818
228	1.000	0.4900	1.132	0.7818
229	1.000	0.5000	1.154	0.7819
230	0.928	0.5000	1.072	0.7819
231	0.827	0.5000	0.954	0.7820
232	0.701	0.5100	0.820	0.7820
233	0.595	0.5100	0.695	0.7821
234	0.504	0.5200	0.597	0.7821

225	0.953	0.4600	1.032	0.7973
226	0.967	0.4800	1.090	0.7973
227	0.994	0.4900	1.143	0.7974
228	1.000	0.4800	1.123	0.7974
229	1.000	0.5000	0.206	0.7974

APPENDIX B

The laboratory x-ray characterisation of the BCS crystals

The bent crystals were produced by gluing thin slices of germanium to titanium substrates previously ground to a concave cylinder. After gluing, the crystal shapes were measured at NIST to determine the resultant curvature. Rather than assuming that a perfect cylinder had been achieved, each crystal was carefully measured using x-rays at a series of closely spaced points over its surface. At each point the direction of the normal to the crystal planes was determined relative to that at crystal centre. The result is a table of positions and angles that describe the crystal curvature in detail, as seen by the x-rays. Interpolation in this table allows us to model the crystal more exactly by following the local direction of the crystal planes all over the crystal surface.

To make the measurements, the crystal under test was placed at the position of the second crystal in a double crystal x-ray spectrometer in the (1 -1) orientation (see figure B1).The source was Cu Kα radiation produced by an x-ray tube and the first crystal was a flat Ge (220) crystal of good quality. A fine slit (0.004 × 1.0 cm^2) was placed between the two crystals so that only a small region of the crystal was illuminated by the parallel monochromatic radiation emerging from the flat crystal. The crystal being tested was

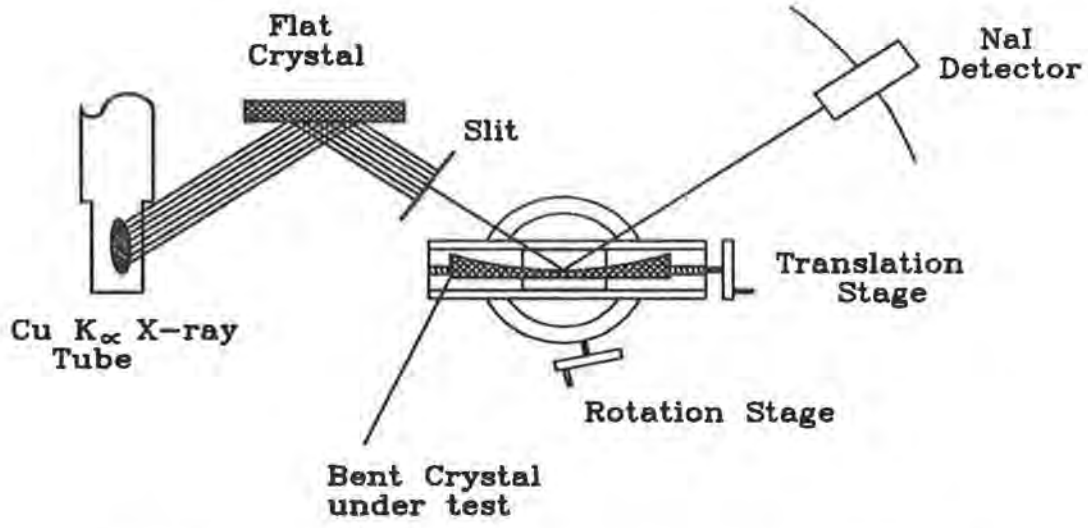

Figure B1. Schematic of the crystal curvature measurement set-up

carried on a translation stage which was itself mounted on a precise rotary stage. This enabled the illuminated spot to be moved about over the entire surface of the crystal.

The centre of the crystal under test was placed on the rotation axis of the rotary stage and a NaI scintillation counter accurately placed in the reflected beam. A flat reference mirror was attached to the crystal so that its angle could be carefully tracked by an autocollimator. Once the "zero" position was established, the crystal was translated to a new position (x) and rotated until the reflected beam again peaked in the NaI detector This rotation angle, read from the precision rotation stage, is the angle of the crystal planes at x relative to those at crystal centre. At each point, the autocollimator was used to re-zero the rotation stage so that any error due to curvature of the translation stage was removed. The angular accuracy of the individual measurements was about 2 arc seconds. Each crystal was measured in three strips, one at the centre of the crystal, one ~1 cm above centre, and one ~1 cm below centre. Measurements were made every ~2 mm along the length of the crystal in these strips.

These data were used to construct tables for the crystal modelling that established the theoretical dispersion and sensitivity of the BCS. The x co-ordinates of the individual data points had to be corrected by a small factor made necessary by the fact that the point of intersection of the x-ray beam with the crystal surface moves away from the rotation axis as the curved crystal is translated away from the central point. The cause of this shift is the fact that the translation stage was mounted on top of the rotary stage. Figure B2 is a

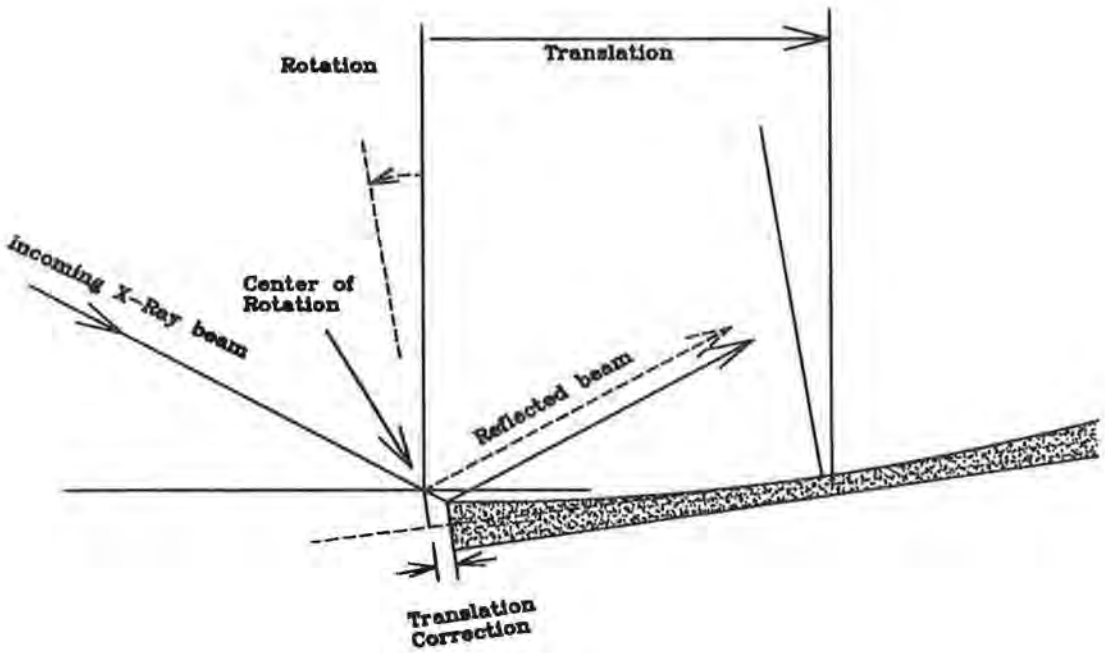

Figure B2. Schematic of crystal translation correction

schematic illustrating this correction. The correction Δx is a shift to the right (in figure B2). As the crystal was set up on the stage for measurement at NIST, it was translated until the ends of the crystal were found (when the x-ray signal fell off) and the midpoint of these two positions set as the zero of the x scale. As both end points are found shifted to the right by Δx, the physical centre of the crystal is located to the left of x=0 by Δx. At any position x relative to the crystal centre, the actual correction Δx is approximately proportional to $| x^2/R |$ (where R is the crystal radius of curvature). The actual transcendental equations were solved precisely by computer iteration. For the BCS crystal radii, the size of the correction is of the order of 1% at the crystal ends. The NIST tables were corrected, with a new scale $X = x - \Delta x$ generated such that $X = 0$ was the physical centre of the crystal and the crystal normal direction at that point was the zero angle to which all other angles were related. The modified tables served as input to later calculations (see Appendix A). Figure B3 is a plot of the deviations of the crystal normal directions from those of a perfect cylindrically bent crystal for each channel.

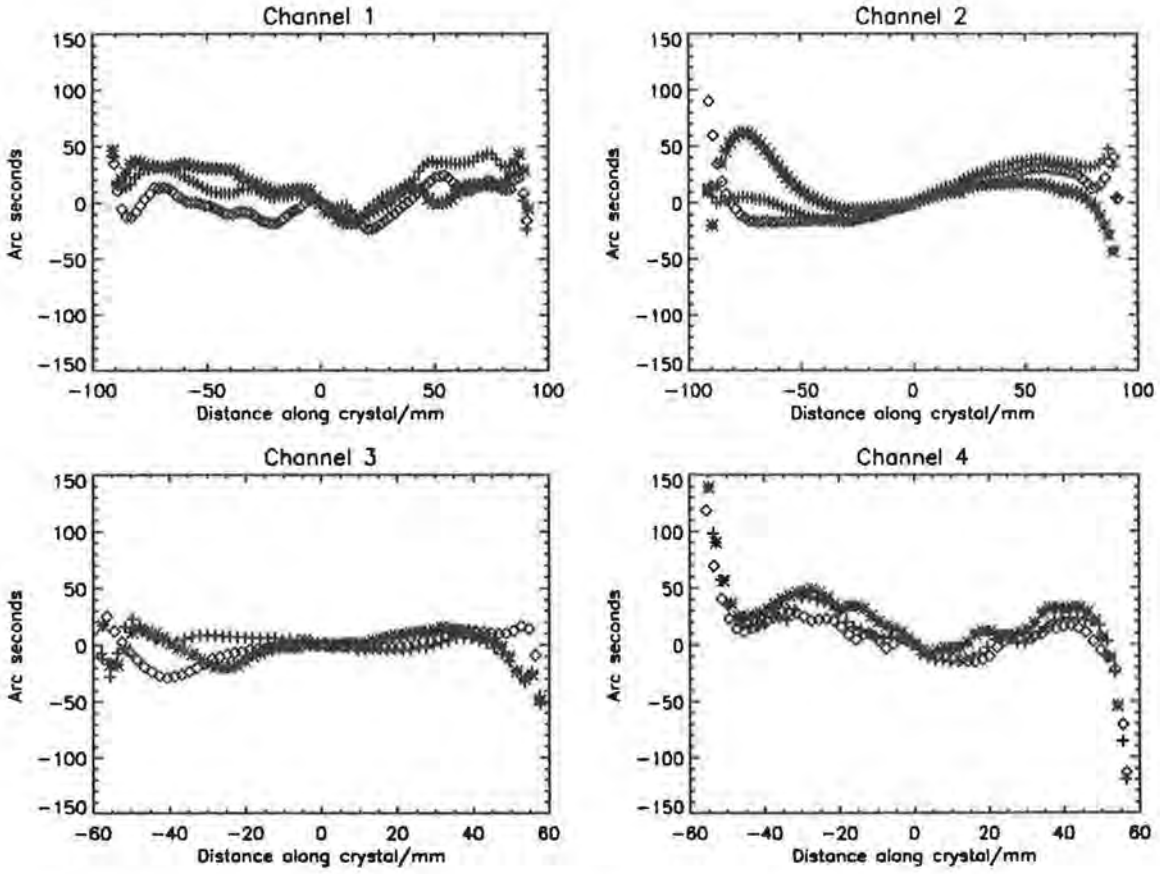

Figure B3. Crystal curvature variations as a function of distance. Plotted are the deviations from circular shape in arc seconds for the three sets of measurements across each crystal.

APPENDIX C

Measurements of the Yohkoh BCS F1 and F3 beryllium window transmissions

These measurements were done in the Rutherford Appleton Laboratory end-to-end test apparatus using molybdenum Lα radiation. The source was run at 16 kV and 5 mA with slits 3 and 4 set at 1 mm wide. The windows tested were from detectors F1 and F3 while they were being refurbished for use as flight spares. The windows had been used on these detectors before they failed and were still brazed into the detector top assemblies. This assembly was placed in a jig in the BCS mounting box. By moving the Unidex x axis the window could be scanned across the x-ray beam. The windows were mounted vertically with the pump stem at the bottom and on the east side. The position nomenclature is given below and was as for the position linearity measurements. The positions of the strengthening ribs on the windows were avoided when taking data.

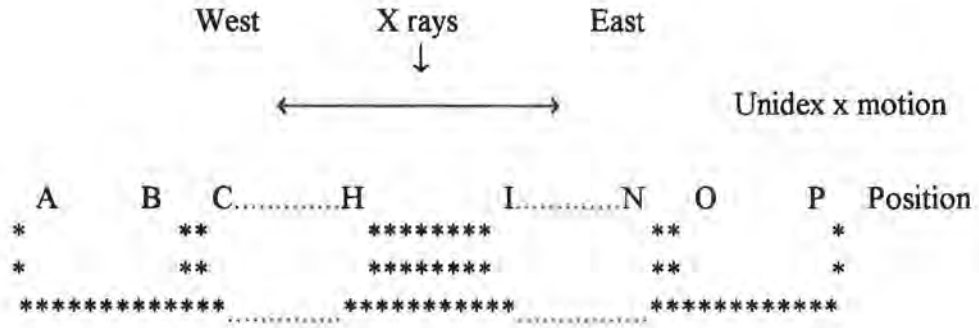

The monitor detector was masked so that 4 cm in height at the position of the window would be illuminated. Two traverses were done for each of the two windows measured, illuminating the "top" or "bottom" of the window depending on the presence of the spacer. The count rate on the monitor with the window out was around 35 counts/second and the integration time was set to 100 seconds, giving better than 1% statistics for both the window out (I_O) and window in (I) measurements.

Tables C1 and C2 give the results of the measurements for windows F3 and F1 respectively. The measurements were done in the sequence of window out, window in, new window position, window in, window out, new window position and so on. The background signal (i.e. the signal with no x-rays incident on the detector and with the window withdrawn) was measured twice for each of the lower and upper window

measurements and the counts in 100 seconds were 73, 57, 84 and 67 for F3 and 59, 45, 82 and 64 for F1. This background was ignored in evaluating the window transmission and its uncertainty. The quoted uncertainties in the transmissions (ΔT) are calculated from the statistical uncertainties in the window out and in measurements. The constancy of the beam can be inferred from the window out measurements and is good. As well as the total counts, the detector gave position spectra which were examined to check the x-ray beam uniformity.

Considering the results for window F3 (table C1) it can be seen that the nominal position and the actual position as used for the measurements differed as the window was moved further to put the relevant area in the x-ray beam. The difference is attributed to the plane of the window not being parallel to the traverse direction. At position P in the lower part of the window there is a blob of solder/flux on the window which accounts for the lower transmission.

Table C1 Results for window F3

	Lower part of window					Upper part of window				
Position (letter, nominal mm)	U'dex posn mm	I_o counts	I counts	T %	ΔT %	U'dex posn mm	I_o counts	I counts	T %	ΔT %
A	-	-	-	-	-	-	-	-	-	
B,0	0	-	14099	37.5	0.4	0	-	12086	34.5	0.4
C,6	6	-	13487	35.8	0.4	6	-	12146	34.6	0.4
D,10	10	37629	13158	35.0	0.4	10	35077	12122	34.6	0.4
E,16	16	-	13694	36.4	0.4	16	-	11325	32.3	0.4
F,20	20	37237	13627	36.6	0.4	20	35042	11369	32.4	0.4
G,26	26	-	14769	39.7	0.4	26	-	11625	33.2	0.4
H,30	30	37795	13305	35.2	0.4	30	34653	10727	31.0	0.4
I,40	42	-	13562	35.9	0.4	42	-	11108	32.0	0.4
J,46	47	37904	13554	35.8	0.4	47	34910	11714	33.6	0.4
K,50	52	-	13697	36.1	0.4	52	-	11838	33.9	0.4
L,56	58	38046	13687	36.0	0.4	57	34570	11781	34.1	0.4
M,60	62	-	13272	34.9	0.4	62	-	11687	33.8	0.4
N,66	67	37731	13740	36.4	0.4	67	34821	11475	33.0	0.4
O,70	72	-	13313	35.3	0.4	72	-	11855	34.1	0.4
P,76	77	38086	11307	29.7	0.4	74?	34484	12106	35.1	0.4

The mean transmission of the lower part of the window, excluding the blob position, is (36.2±1.2)% and for the upper part the mean is (33.5±1.2)%. The uncertainty reflects the spread of the data points as the averaging procedure was unweighted and no account was taken of the uncertainty in an individual measurement. There is a slight difference in

average transmission between the top and bottom of the window. The average of the top and bottom measurements for window F3 is (34.8±1.8)%.

Table C2 Results for window F1

Position (letter, nominal mm)	Lower part of window U'dex posn mm	I_0 counts	I counts	T %	ΔT %	Upper part of window U'dex posn mm	I_0 counts	I counts	T %	ΔT %
A	-	-	-	-	-	-	-	-	-	-
B,0	0	34932	12027	34.4	0.4	0	33780	11316	33.5	0.4
C,6	6	34498	12056	35.0	0.4	6	34483	11278	32.7	0.4
D,10	10	-	12062	35.0	0.4	10	-	11560	33.5	0.4
E,16	16	34562	11820	34.2	0.4	16	34704	11442	33.0	0.4
F,20	20	-	12022	34.8	0.4	20	-	11509	33.2	0.4
G,26	26	34879	11939	34.2	0.4	26	34306	11373	33.2	0.4
H,30	30	-	11818	33.9	0.4	30	-	11528	33.6	0.4
I,40	42	34838	11248	32.3	0.4	42	34423	10784	31.3	0.4
	43	-	11920	34.2	0.4	43	-	11577	33.6	0.4
	43	-	11716	33.6	0.4	-	-	-	-	
J,46	46	-	11845	34.0	0.4	46	-	11776	34.2	0.4
	-	-	-	-	-	47	-	11168	32.4	0.4
K,50	52	35074	11471	32.7	0.4	51	34694	11448	33.0	0.4
	53	-	11874	33.9	0.4	-	-	-	-	-
L,56	56	-	11820	33.7	0.4	57	-	11617	33.5	0.4
M,60	62	34950	11573	33.1	0.4	62	34929	11339	32.5	0.4
	63	-	12063	34.5	0.4	-	-	-	-	-
N,66	67	-	11859	33.9	0.4	67	-	11445	32.8	0.4
O,70	72	34650	11597	33.5	0.4	72	34934	11702	33.5	0.4
	73	-	11995	34.6	0.4	-	-	-	-	-
P,76	76	-	11771	34.0	0.4	76	-	11679	33.4	0.4

Window F1 (table C2) was better placed on the translation box because the differences between the nominal and actual positions do not vary as they did for window F3. The average transmission for the lower part is (34.0±0.7)%. At position I the same part of the window was measured twice and the results agree within the statistical uncertainties. For the upper part of the window the average transmission is (33.1±0.7)%. The averages for the lower and upper parts agree within the uncertainties. The average transmission for window F1 is (33.4±1.2)%.

The cross section for the photo-absorption of beryllium has been given by Henke et al. (1982, Atomic Data and Nuclear Data Tables, **27**, 1-144). At the wavelength of Mo Lα

(2293.2 eV) the mass absorption coefficient $\mu = 46.1$ cm^2/g while the density of beryllium is taken as $d = 1.846$ g/cm^3. The transmission, T, is related to the thickness of material L by the usual equation $T = \exp(-\mu \times d \times L)$. Substituting the measured transmissions into this equation gives the thickness of window F3 as 124±4 microns and for F1 as 129±4 microns. The nominal thickness is 125 microns.

Table C3 gives the values of μ in cm^2/g for beryllium obtained by graphical interpolation of Henke's data and are evaluated at the short and long wavelength ends of each of the BCS channels. The percentage transmissions are then given for these values of μ and the density of beryllium given above and assuming that the window thickness is 125 microns. Also given are the average of the high and low transmissions (T_{av}) and the effective transmissions (T_{ef}) which includes the allowance for the window throughput factor (0.84) which corrects for the effect of the opaque strengthening bars.

Table C3

Channel	μ(lo)	μ(hi)	T(lo)	T(hi)	T_{av}	T_{ef}
1 (Fe XXVI)	1.17	1.25	97.3	97.2	97	82
2 (Fe XXV)	1.37	1.42	96.9	96.8	97	81
3 (Ca XIX)	7.8	8.2	83.5	82.8	83	70
4 (S XV)	33	34	46.7	45.6	46	39

Conclusions

Although the transmissions of the windows fitted to the flight detectors have not been measured, they are from the same source as the ones tested. Taking the present measurements to imply that the thickness of the windows is 125 microns is known to say ±3% means that the effective transmission quoted for channel 4 of 39% is known to 4%, i.e. (39±2)%. For channel 3 the effective transmission comes to (70±1)% while for channels 1 and 2 the uncertainty does not affect the quoted values.

Acknowledgements

M. W. Trow is thanked for his assistance in making the measurements.

APPENDIX D

The location of the detector bins and the effect of unwanted weld material

The position linearity of each of the BCS detectors was measured using the end-to-end test apparatus. From these measurements it was possible for each channel to determine the start position of each of the bins with respect to the edge of the detector quartz plate.

When the beryllium window was welded to the stainless steel body of the detector, some of the welding material was deposited on the window and could not be removed. From photographs taken of the welded detector windows it was possible to establish the reduction in window transmission caused by the presence of this material. This weld area factor was measured as function of the distance from the edge of the beryllium window. These data were used to establish the weld area factors for each channel for all bins which could be illuminated by x-rays transmitted by the window.

Figures A1 to A4 in Appendix A of this report show the weld area factors and the bin widths as a function of detector bin number for channels 1 to 4 respectively. Table A2 in Appendix A gives the data used to produce the figures.

Acknowledgements

A. Fludra, A. T. Phillips and M. W. Trow are thanked for supplying tables of detector bin number and bin start position and the results of the weld transmission measurements.

APPENDIX E

Measurements of the Yohkoh BCS thermal filter transmissions

1. Introduction

The thermal filters consist of kapton of 10 micron nominal thickness coated with an aluminium film 1000Å thick. They provide an x-ray window for the spectrometers and protect them from solar heat and the space environment. The filter x-ray transmission measurements were done in the end-to-end test apparatus as part of the early commissioning work.

2. Measurements of thermal filter transmission

A sulphur doped anode was used to produce S Kα line radiation. This wavelength is very close to the wavelength range for Channel 4 (S XV) and it is for this channel that the filters are most absorbing. The Spellman power supply was run at 16 kV and 2.5 mA. Between the source and the channel-cut crystal were slits 1 and 2 each 0.5 mm wide and 50 mm long, while between the channel cut crystal and the filters were slits 3 and 4 again each being 0.5 mm wide and 50 mm long. The distances between the various items are given in table E1. About 50 mm after the crystal toward slit 3 a copper mask 40 mm high and 40 mm wide was used to stop radiation which may have passed over the crystal rather than through it. The position-sensitive detector was placed after the filter under test. The detector window was fitted with a mask with an aperture 44 mm high by 0.5 mm wide, the centre of the mask being on the centre line of the x-ray beam. The detector was run at 1600 V with a mixture of 7.5% methane and 92.5% argon.

Table E1. Distances between components of the x-ray test apparatus

Components			Distance/mm
Anode	-	1st slit	70
1st slit	-	2nd slit	120
2nd slit	-	Crystal	140
Crystal	-	3rd slit	500
3rd slit	-	4th slit	330
4th slit	-	Filter	800
Filter	-	Detector	400

Twelve filters mounted in holders were supplied for testing. Filters number 1, 5, 9 and 12 had their transmissions measured. These particular filters were chosen to give at least one from each of the groups of four which had been aluminised as a batch. The filters were supplied glued to frames 140 mm by 152 mm which were mounted in the translation box with the long side vertical. This side also had screw holes to facilitate mounting. The number of the filter was marked in a corner of the frame and this corner was placed on the bottom left looking in the direction of the x-ray source from the filter as indicated by N on the diagram below. (This diagram is not to scale.)

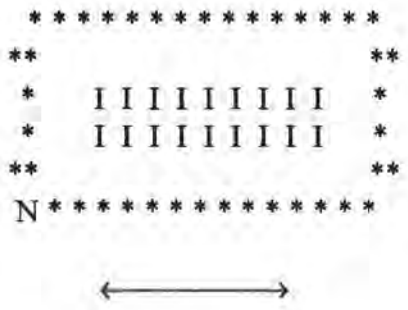

Two sets of measurements were done on each filter. They were made on the upper and lower halves of the filter for nine positions each 10 mm apart horizontally as depicted on the diagram. The positions are numbered from 1 to 9 from left to right on the diagram. As the x-ray beam was 44 mm high at the detector, this meant that there was a border of about 15 mm all round the edge of the filter which was not measured. The size of the flight filter holders is smaller (85 mm by 100 mm) than the filter frame and most of the unmeasured area would not be used for the flight filters.

By moving the translation box to one side to the "home" position using the Unidex motion controller, it was possible to make the filter out measurement (I_0). Tables A2 to A5 give the results of the measurements for the four filters selected. The 'Bgd Home' and 'Bgd Fltr' in these tables are the background signals as measured at the home position and with the filter in with no incident radiation. The counts observed are attributed mainly to cosmic rays.

The counts shown in tables E3 - E5 were obtained over the whole beam. The proportional counter had position sensitivity and this facility was used to examine the uniformity of the x-ray beam along its 44 mm height. The position resolution of the counter was about 1 mm. Because the total counts were subdivided into 512 bins, the statistics were not so good for these data. However, the data did show that the x-ray beam was fairly uniform, the most intense parts being within a factor of two of the least intense parts. Separate microscopic examination of the filters revealed many small pinholes in the aluminium coating. These have negligible total area. Since the aluminium is a small part of the filter's attenuation factor, the pinholes have no effect on the transmission of the filters or the performance of the spectrometers.

Table E2 Results for Filter No 1

	Upper part of filter			Lower part of filter		
Position	Counts	T(%)	ΔT(%)	Counts	T(%)	ΔT(%)
Home	10075	-	-	10914	-	-
1	6348	62.3	1.0	6862	62.2	1.0
2	6232	59.3	1.0	6761	60.2	1.0
Home	10384	-	-	11116	-	-
3	6171	58.7	1.0	6844	60.9	1.0
4	6235	59.6	1.0	6794	60.7	1.0
Home	10327	-	-	11068	-	-
5	6387	61.1	1.0	6849	59.6	1.0
6	6280	58.0	1.0	6893	59.2	1.0
Home	10696	-	-	11522	-	-
7	6239	57.6	1.0	7089	60.9	1.0
8	6255	58.2	1.0	6991	60.7	1.0
Home	10610	-	-	11401	-	-
9	6283	58.5	1.0	7135	62.0	1.0
Bgd Home	254	-	-	208		-
Bgd Fltr	229	-	-	198	-	-

Table E3 Results for Filter No 5

	Upper part of filter			Lower part of filter		
Position	Counts	T(%)	ΔT(%)	Counts	T(%)	ΔT(%)
Home	10260	-	-	11142	-	-
1	6190	59.6	1.0	6901	61.2	1.0
2	6419	60.8	1.0	6880	60.6	1.0
Home	10443	-	-	11224	-	-
3	6267	59.3	1.0	6770	59.6	1.0
4	6278	59.9	1.0	6809	59.6	1.0
Home	10369	-	-	11290	-	-
5	6303	60.1	1.0	6724	58.8	1.0
6	6319	59.4	1.0	6974	59.4	1.0
Home	10512	-	-	11598	-	-
7	6357	59.8	1.0	7126	60.8	1.0
8	6327	59.8	1.0	7032	59.6	1.0
Home	10452	-	-	11672	-	-
9	6298	59.6	1.0	6999	59.3	1.0
Bgd Home	220	-	-	238	-	-
Bgd Fltr	203	-	-	222	-	-

Table E4 Results for Filter No 9

	Upper part of filter			Lower part of filter		
Position	Counts	T(%)	ΔT(%)	Counts	T(%)	ΔT(%)
Home	11290	-	-	10544	-	-
1	7059	62.2	1.0	6686	63.0	1.0
2	6917	59.4	1.0	6437	59.8	1.0
Home	11574	-	-	10666	-	-
3	6944	59.6	1.0	6567	61.1	1.0
4	6996	58.6	1.0	6605	61.1	1.0
Home	11866	-	-	10723	-	-
5	7145	59.9	1.0	6472	59.9	1.0
6	6986	57.5	1.0	6673	62.3	1.0
Home	12061	-	-	10642	-	-
7	7187	59.2	1.0	6607	61.6	1.0
8	7156	58.8	1.0	6509	59.5	1.0
Home	12102	-	-	10843	-	-
9	7063	58.0	1.0	6467	59.1	1.0
Bgd Home	210	-	-	219	-	-
Bgd Fltr	167	-	-	184	-	-

Table E5 Results for Filter No 12

	Upper part of filter			Lower part of filter		
Position	Counts	T(%)	ΔT(%)	Counts	T(%)	ΔT(%)
Home	10903	-	-	10694	-	-
1	6747	61.3	1.0	6833	63.5	.0
2	6738	59.4	1.0	6830	60.0	1.0
Home	11220	-	-	11313	-	-
3	6762	59.6	1.0	6878	60.4	1.0
4	6641	57.5	1.0	6832	59.8	1.0
Home	11419	-	-	11349	-	-
5	6714	58.2	1.0	6937	60.7	1.0
6	6732	59.3	1.0	6851	57.7	1.0
Home	11229	-	-	11795	-	-
7	6820	60.1	1.0	6793	57.2	1.0
8	6668	57.3	1.0	6813	57.7	1.0
Home	11504	-	-	11725	-	-
9	6813	58.6	1.0	7143	60.5	1.0
Bgd Home	203	-	-	209	-	-
Bgd Fltr	190	-	-	171	-	-

The quality of the results depends on the stability of the x-ray beam as there was no independent x-ray monitor. The stability of the x-ray power supply was excellent. The filter out results have 1% counting statistics. Examination of the filter out counts in tables E2 to E5 show that some of the variations in transmission are consistent with beam fluctuations. However, it should be noted that variations in transmission are quite small. Table E6 gives the average percentage transmission for the upper and lower parts of each filter and the average of these for each filter. The averages are unweighted.

Table E6

Filter no.	Average for upper part	Average for lower part	Average for filter
1	59.2±1.6	60.7±1.0	60.0±1.5
5	59.8±0.4	59.9±0.8	59.9±0.6
9	59.2±1.3	60.8±1.3	60.0±1.5
12	59.0±1.3	59.7±2.0	59.4±1.7

The average transmission for the four filters is (59.8±1.5)%. Essentially, the thermal filter transmission at the sulphur Kα wavelength is (60±2)%.

3. Application of measurements to the BCS filters

The manufacturer's tolerance on the 10 micron nominal thickness for the kapton was ±30%. An attempt to derive the thickness by weighing the kapton knowing its area and density was unsatisfactory because the static charge on the sheet interfered with the weight measurement. Measuring a stack of 8 sheets gave a thickness of 13 microns which is at the upper end of the given tolerance band. The nominal thickness of the aluminium was 1000Å. The kapton was coated in batches of 4, with 1 - 4 in batch 1 etc. with the numbers corresponding to those used above. The coating process was monitored, readings being reported from a quartz microbalance coating monitor which weighed the deposited aluminium. The operator reported seeing the coating appear before the microbalance read above zero. Hence there is at least a zero offset in the numbers and the reported thicknesses should be used cautiously. For completeness the reported thicknesses of batches 1, 2 and 3 are 925.9Å, 829.6Å and 859.3Å respectively

In applying the present measurements to estimate the absorption of the thermal filters over the wavelength ranges of the BCS channels the difficulty is that one measurement of absorption has been made but there are two absorbers present, aluminium and kapton. Cross sections for photoabsorption have been given by Henke et al. (1982, Atomic Data and Nuclear Data Tables, **27**, 1 - 144). From these data, by graphical interpolation where necessary, the values of the mass absorption coefficient μ in cm^2/g were obtained at the wavelength of the S Kα line and for the high and low wavelength limits of the four BCS channels, given in table E7. For kapton the formula weight 69.1% C, 7.3% N, 2.6% H and

20.9% O was used. The densities (d) of kapton and aluminium are taken as 1.47 and 2.70 g/cm^3 respectively.

Table E7 Tables of μ (cm^2/g)

Channel	1 (Fe XXVI)		2 (Fe XXV)		3 (Ca XIX)		4 (S XV)		S Kα
W'l'gth (Å)	1.76	1.89	1.83	1.89	3.16	3.19	5.01	5.12	5.37
μ (Al)	68.0	73.0	76.0	82.5	340	375	1300	1400	1560
μ (kapton)	8.67	9.19	9.63	10.48	52.2	56.3	206	217	257

Taking the reported thickness of aluminium as a minimum, the transmission factors $F = I/I_0 = \exp(- \mu \times d \times L)$ for thicknesses L of aluminium of 900Å, 1000Å and 1200Å are 0.963, 0.959 and 0.951 respectively at the wavelength of the sulphur Kα line. 1200Å is considered a reasonable upper limit for the thickness of aluminium as the coating was carried out at a well used and tried facility where gross error in filter coating would have been found. Table E8 shows the transmission factors for various thicknesses of kapton and for combinations of these with the three thicknesses of aluminium.

Table E8

Kapton thickness (microns)	F	F×0.963	F×0.959	F×0.951
14	0.589	0.567	0.565	0.560
13.5	0.600	0.578	0.576	0.571
13	0.612	0.589	0.587	0.582
12.5	0.624	0.601	0.598	0.593
12	0.635	0.612	0.609	0.604
11.5	0.648	0.624	0.621	0.612
11	0.660	0.636	0.633	0.628
10	0.680	0.655	0.652	0.647

From inspection of table E8 the measurements of filter transmission are consistent with a thickness of kapton between 13.5 and 11.5 microns with the aluminium being up to 1200A thick. Table E9 gives the percentage transmission at the high and low wavelengths for each of the BCS channels for filters with these ranges of thicknesses.

Table E9 Filter Transmission

Channel	4	3	2	1
Transmission (%)				
at high w'l'gth	65±2	89±1	98	98
at low w'l'gth	66±2	90±1	98	98

4. Conclusions

From measurements of the transmissions of four (nos 1, 5, 9 and 12) of a batch of twelve thermal filters the transmission of the BCS flight filters has been estimated. For channels 1 and 2 the transmission is (98.0±0.5)%, for channel 3 (90±2)% and channel 4 (66±3)%. Note that filters 5 and 6 are currently flight filters, the former being used with BCS-A and the latter with BCS-B. Filters 1 and 3 are designated as the flight spares.

5. Acknowledgements

R. W. Hayes is thanked for his advice and help.